Towards Continuous-Variable Quantum Neural Networks for Biomedical Imaging

Authors
M. Sc. Daniel Alejandro Lopez
Dr. Oscar Montiel
Dr. Miguel Angel Lopez
Dr. Oscar Castillo

ICE-10, Valencia, Spain, October 21st, 2025

Content

1.- Introduction

AI for Medical Imaging: Progress and Limitations

- AI, has revolutionized medical image analysis [1–3].
- However, these models rely on **large datasets and heavy computation**, limiting their scalability and interpretability [4].
- **Quantum computing** emerges a new paradigm to process information more efficiently [5].

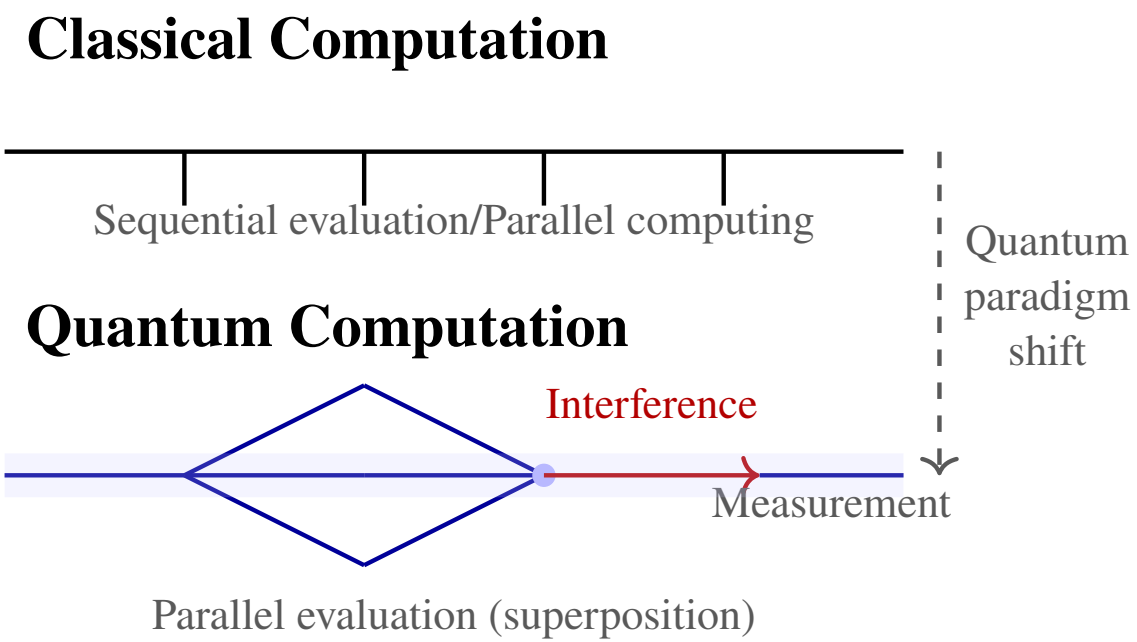

Figure 1: Computation paradigm features and shift.

Quantum AI: Paradigms and Gaps

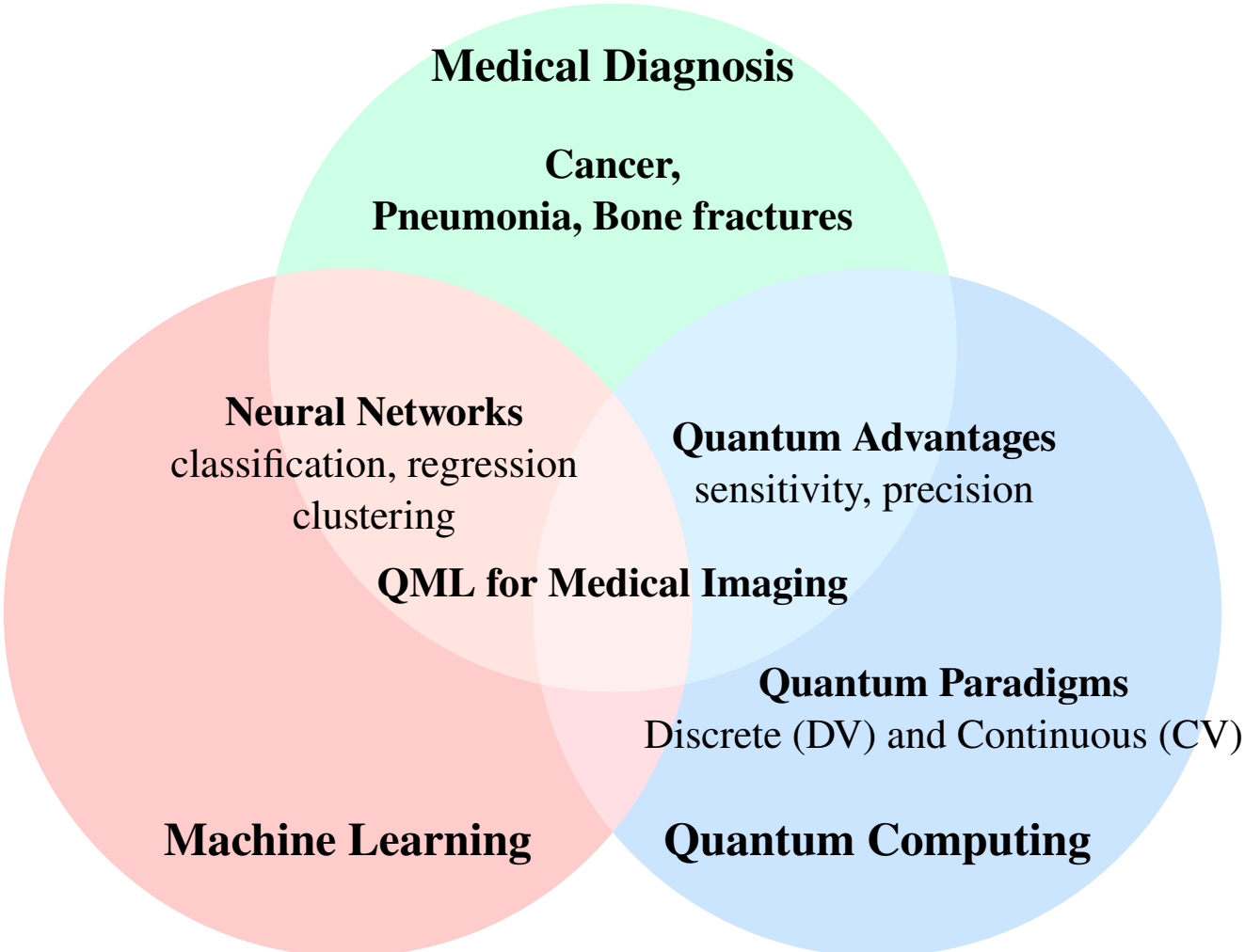

Figure 2: Intersection of disciplines highlighting the research gap in quantum-enhanced medical diagnosis.

Our proposal

- Explore **CV-QNNs** for medical image classification.
- Use **Gaussian gates** (D, R, S, BS) to emulate convolutional behavior.
- Evaluate model performance, robustness, and expressiveness against classical and DV quantum counterparts.

Datasets: BreastMNIST, OrganAMNIST, PneumoniaMNIST
Evaluation: Accuracy, F1-score, AUROC, noise robustness, interpretability.

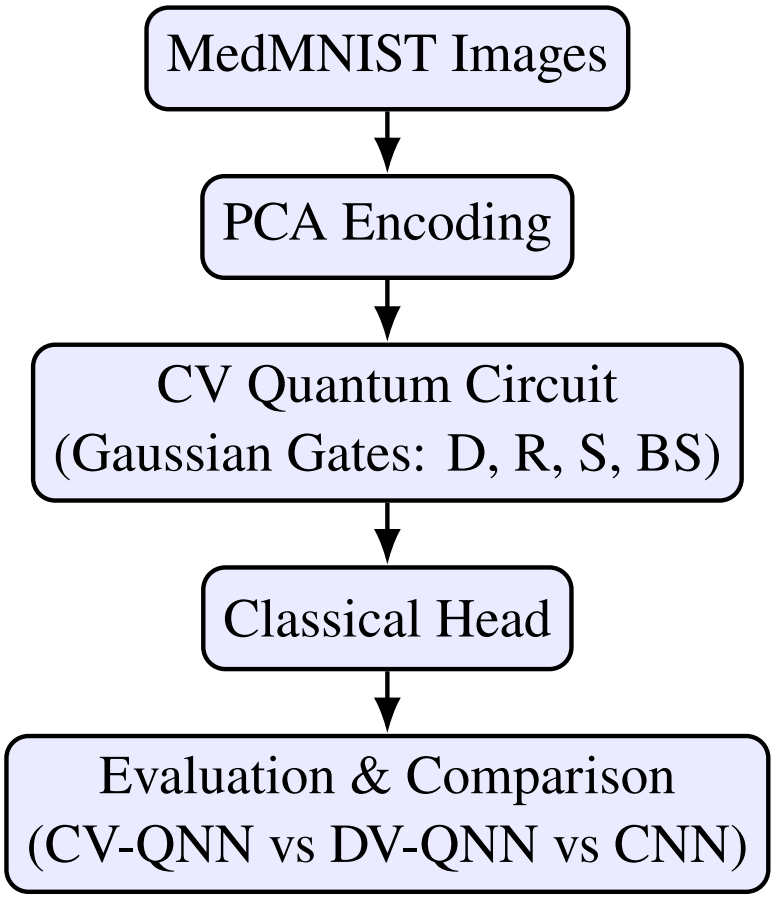

Figure 3: Methodology of the proposed work.

2.- Related work

State-of-the-art of Continuous-Variable QML

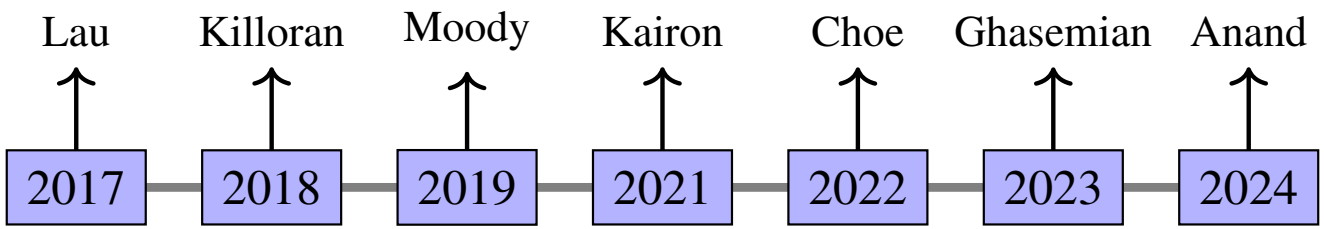

Figure 4: Recent state-of-the-art of Continuous-Variable QML.

State-of-the-art of Continuous-Variable QML

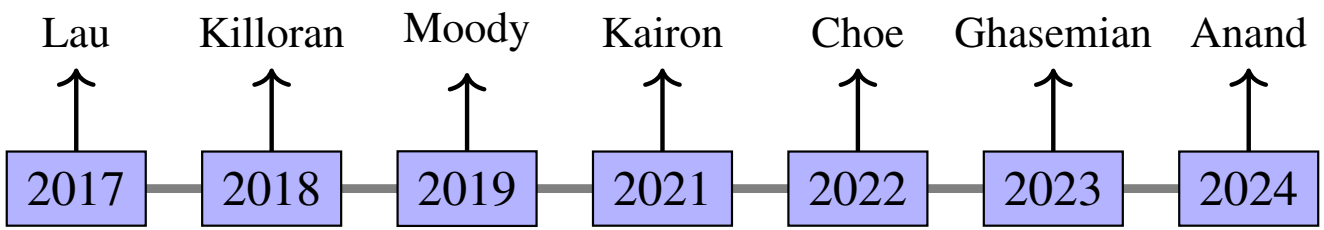

Figure 4: Recent state-of-the-art of Continuous-Variable QML.

- **2017:** Subroutines are generalized for infinite-dimensional systems [6].

State-of-the-art of Continuous-Variable QML

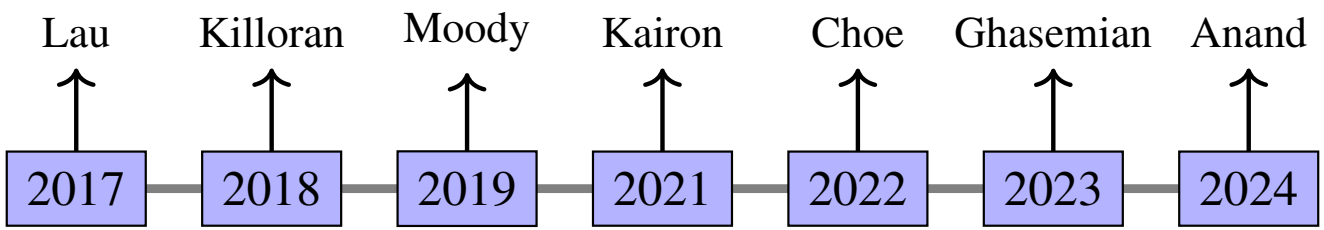

Figure 4: Recent state-of-the-art of Continuous-Variable QML.

- **2017:** Subroutines are generalized for infinite-dimensional systems [6].
- **2018:** First CV neural networks for CV quantum computers [7].

State-of-the-art of Continuous-Variable QML

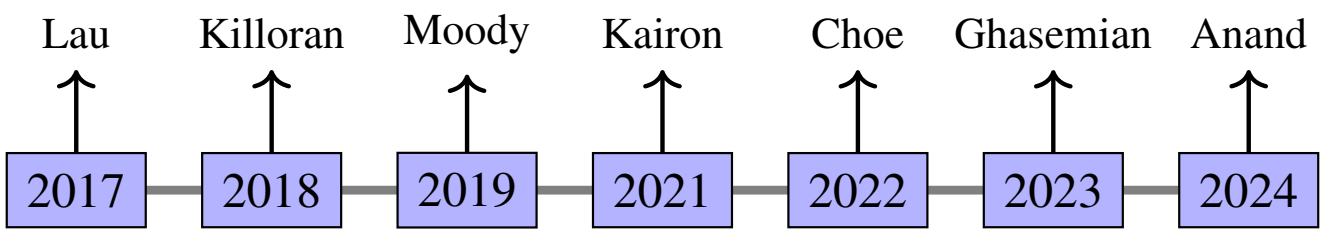

Figure 4: Recent state-of-the-art of Continuous-Variable QML.

- **2017:** Subroutines are generalized for infinite-dimensional systems [6].
- **2018:** First CV neural networks for CV quantum computers [7].
- **2019:** ML and optimization with variable parameters for short-depth photonic circuits [8].

State-of-the-art of Continuous-Variable QML

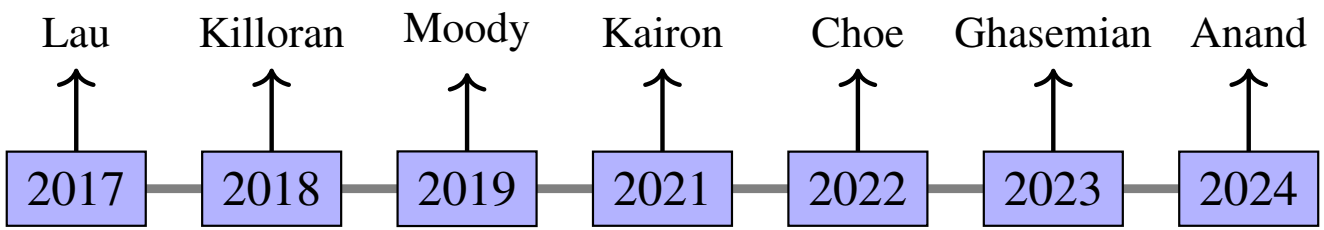

Figure 4: Recent state-of-the-art of Continuous-Variable QML.

- **2017:** Subroutines are generalized for infinite-dimensional systems [6].
- **2018:** First CV neural networks for CV quantum computers [7].
- **2019:** ML and optimization with variable parameters for short-depth photonic circuits [8].
- **2021:** COVID-19 diagnosis through CV QNNs [9].

State-of-the-art of Continuous-Variable QML

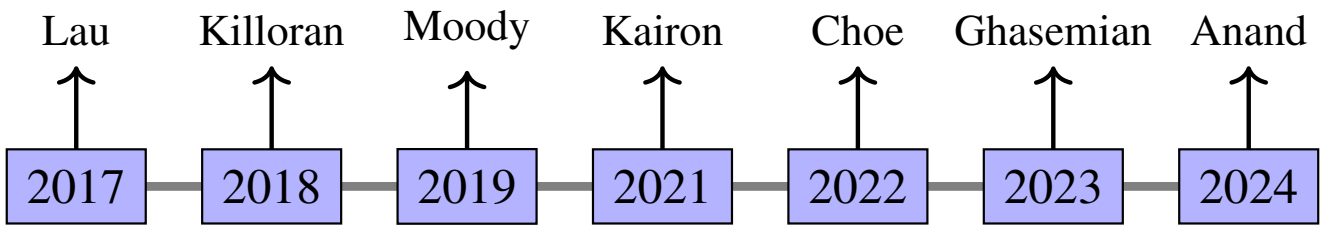

Figure 4: Recent state-of-the-art of Continuous-Variable QML.

- **2017:** Subroutines are generalized for infinite-dimensional systems [6].
- **2018:** First CV neural networks for CV quantum computers [7].
- **2019:** ML and optimization with variable parameters for short-depth photonic circuits [8].
- **2021:** COVID-19 diagnosis through CV QNNs [9].
- **2022:** MNIST classification via CV QNN architecture [10].

State-of-the-art of Continuous-Variable QML

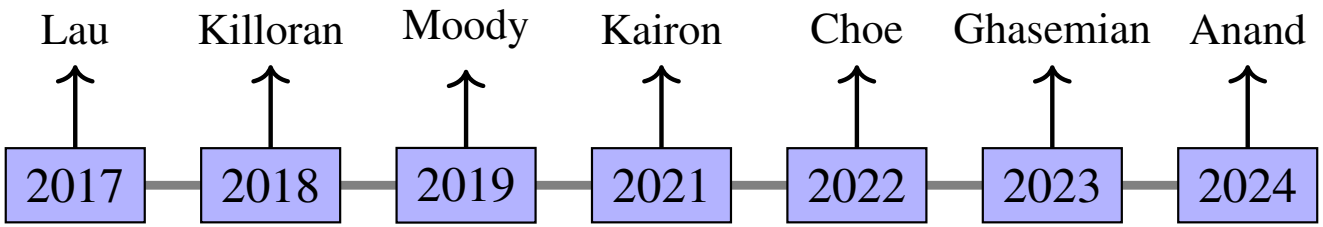

Figure 4: Recent state-of-the-art of Continuous-Variable QML.

- **2017:** Subroutines are generalized for infinite-dimensional systems [6].
- **2018:** First CV neural networks for CV quantum computers [7].
- **2019:** ML and optimization with variable parameters for short-depth photonic circuits [8].
- **2021:** COVID-19 diagnosis through CV QNNs [9].
- **2022:** MNIST classification via CV QNN architecture [10].
- **2023:** Neural network implementations on photonic computers to encode spectral amplitude information [11].

State-of-the-art of Continuous-Variable QML

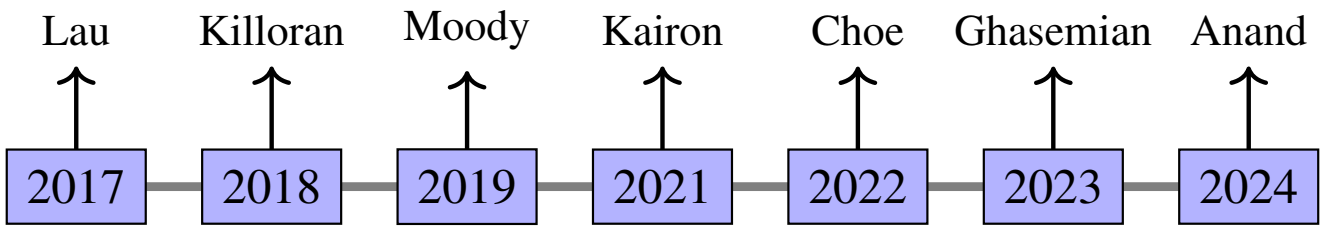

Figure 4: Recent state-of-the-art of Continuous-Variable QML.

- **2017:** Subroutines are generalized for infinite-dimensional systems [6].
- **2018:** First CV neural networks for CV quantum computers [7].
- **2019:** ML and optimization with variable parameters for short-depth photonic circuits [8].
- **2021:** COVID-19 diagnosis through CV QNNs [9].
- **2022:** MNIST classification via CV QNN architecture [10].
- **2023:** Neural network implementations on photonic computers to encode spectral amplitude information [11].
- **2024:** Time-series forecasting comparison between quantum CV, DV and classical approaches [12].

3.- Methodology

Data preparation

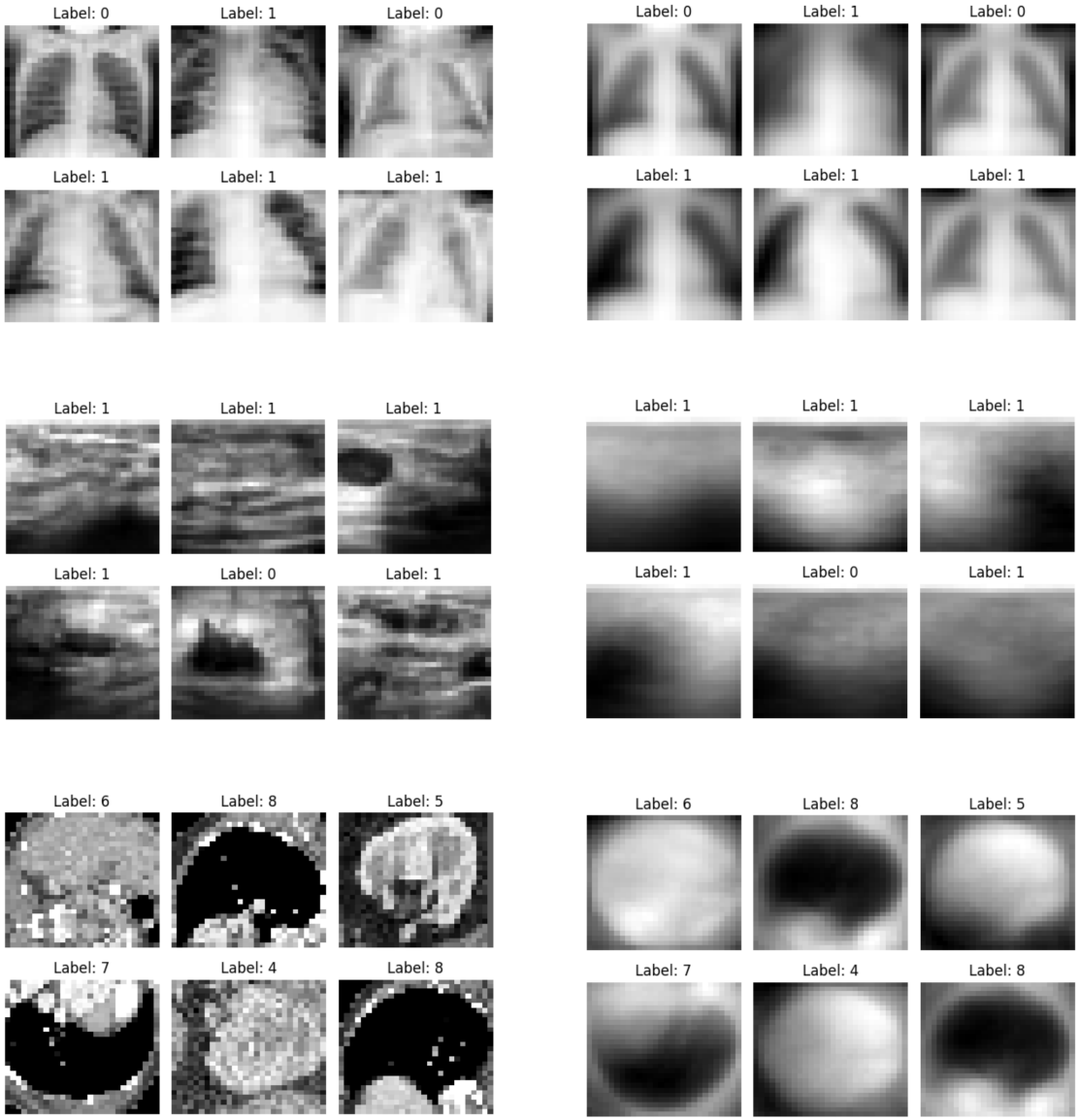

Figure 5: Comparison between original and PCA-reconstructed images.

Data dimensionality reduction

Table 1: Dimensionality reduction using PCA across MedMNIST datasets.

Dataset	Task	Dimensions	No. Samples	PCA	Var.
Breast	Binary	(28, 28, 1)	546	4	~60%
Organ	Multiclass	(28, 28, 1)	10368	4	~48%
Pneumonia	Binary	(28, 28, 1)	4708	4	~60%

Continuous-Variable quantum neural network

Continuous-Variable quantum neural network

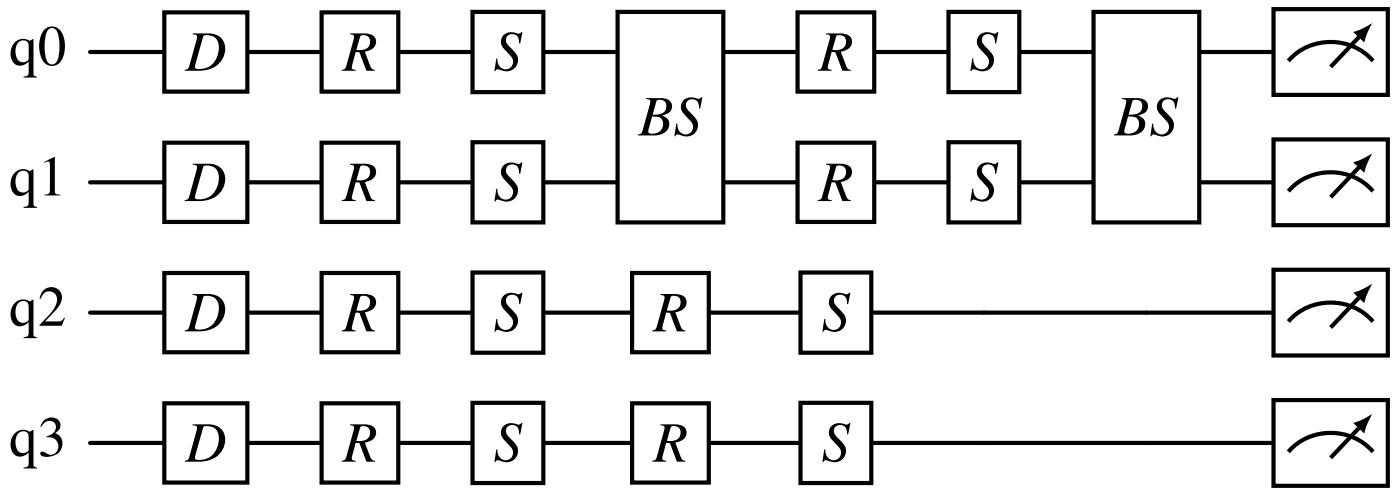

Figure 6: The proposed 4-mode Continuous-Variable (CV) quantum circuit.

Displacement gate

$$D(\alpha) = \exp\left(\alpha\hat{a}^{\dagger} - \alpha\hat{a}\right), \tag{1}$$

Continuous-Variable quantum neural network

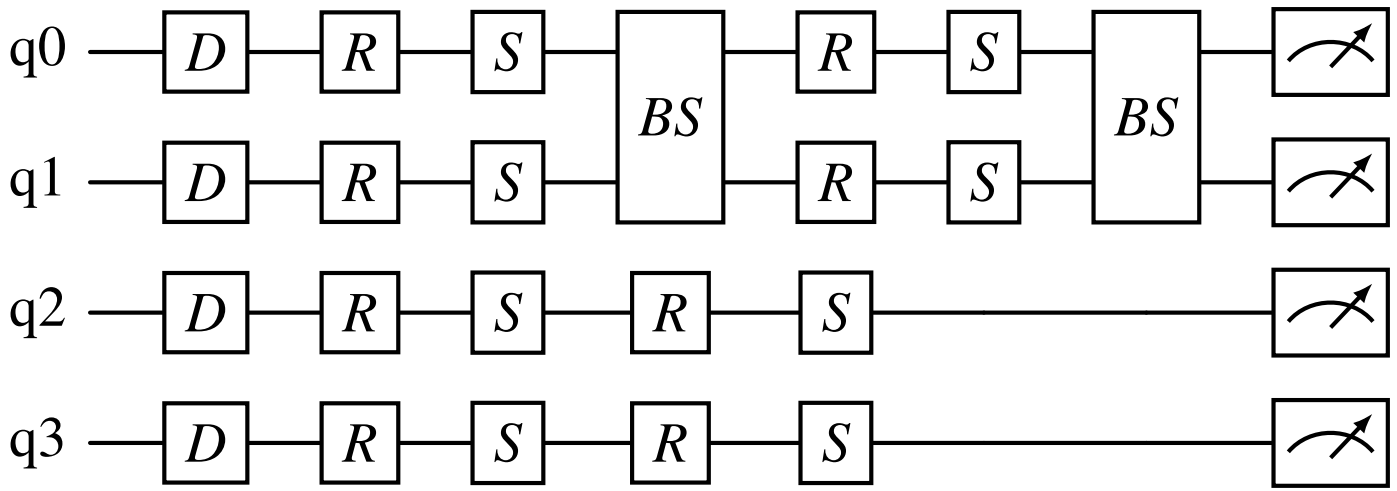

Figure 6: The proposed 4-mode Continuous-Variable (CV) quantum circuit.

Rotation gate

$$R(\phi) = \exp\left(i\phi\hat{a}^{\dagger}\hat{a}\right), \tag{2}$$

Continuous-Variable quantum neural network

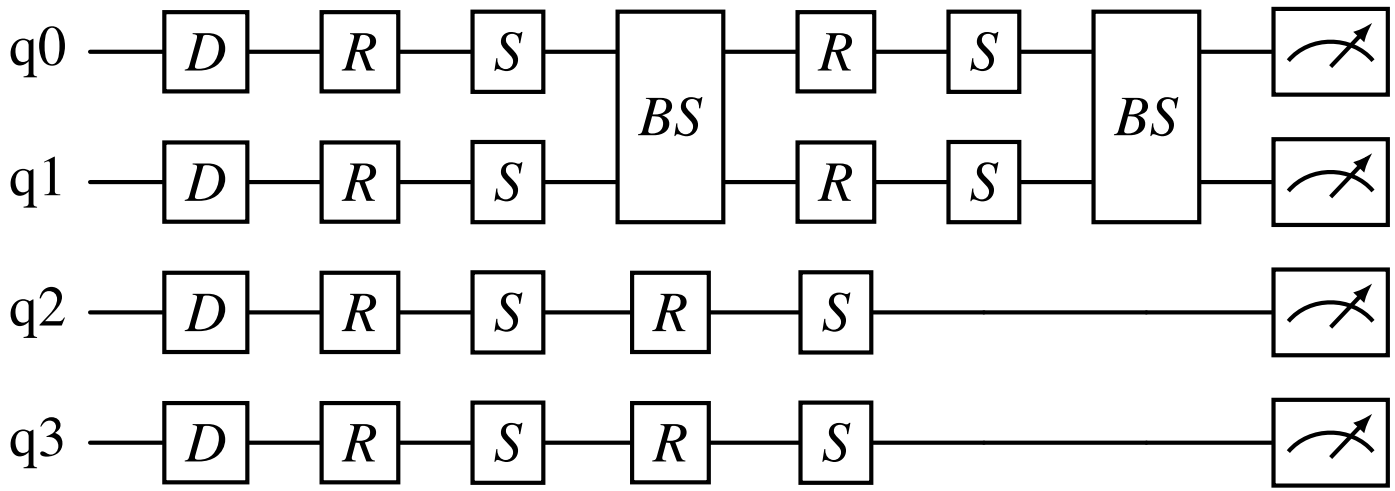

Figure 6: The proposed 4-mode Continuous-Variable (CV) quantum circuit.

Squeezing gate

$$S(r) = \exp\left[\frac{1}{2}r\left(\hat{a}^2 - (\hat{a}^\dagger)^2\right)\right], \tag{3}$$

Continuous-Variable quantum neural network

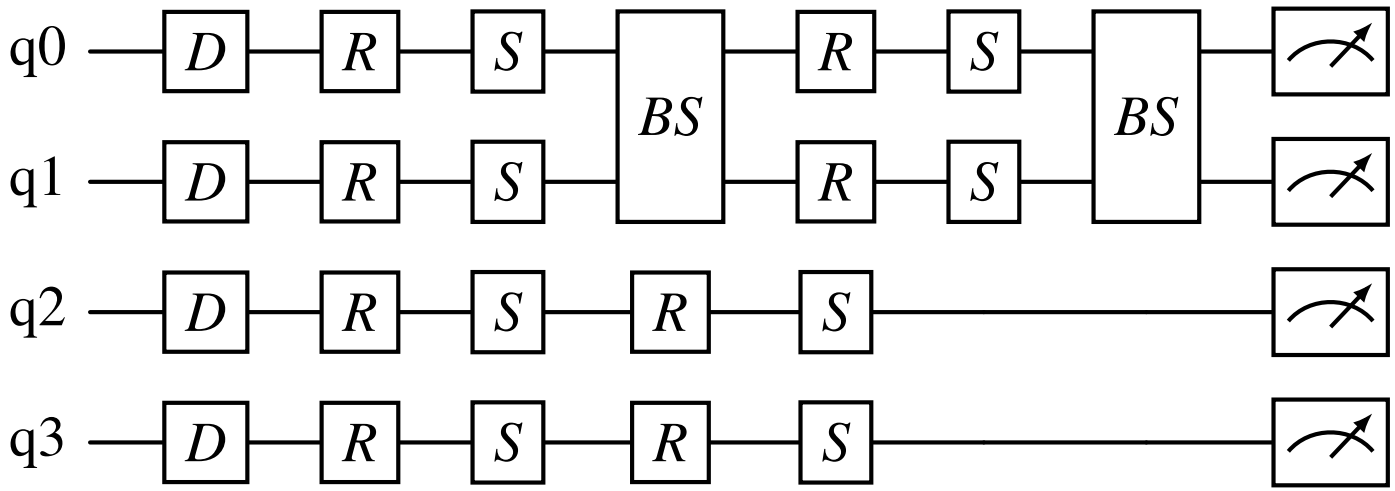

Figure 6: The proposed 4-mode Continuous-Variable (CV) quantum circuit.

Beamsplitter gate

$$BS(\theta, \phi) = \exp\left[\theta\left(e^{i\phi}\hat{a}_1^\dagger \hat{a}_2 - e^{-i\phi}\hat{a}_1 \hat{a}_2^\dagger\right)\right], \tag{4}$$

Continuous-Variable quantum neural network

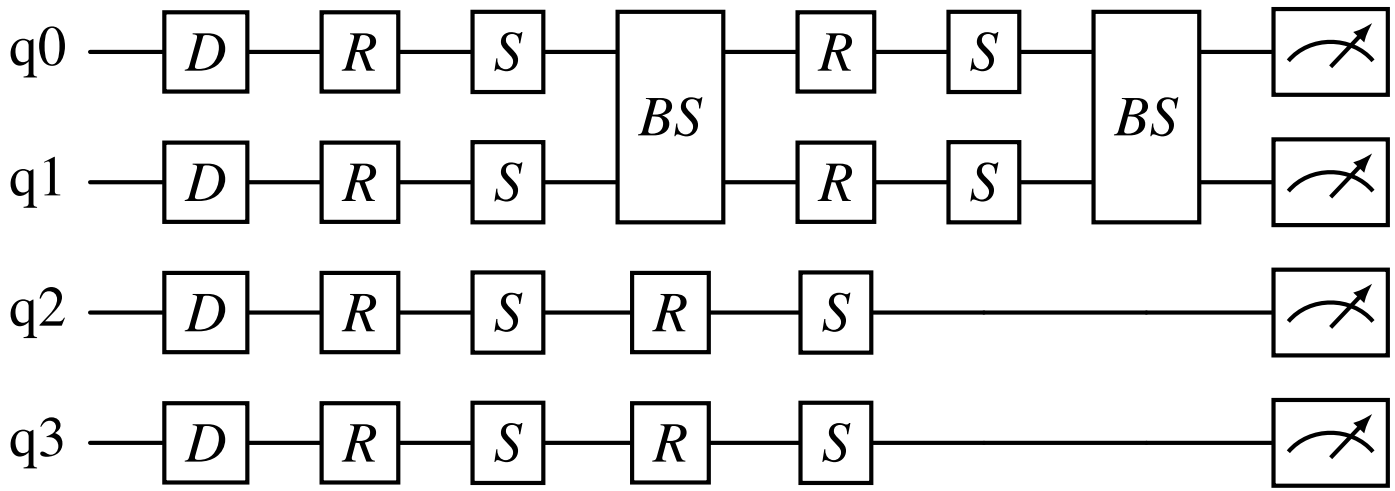

Figure 6: The proposed 4-mode Continuous-Variable (CV) quantum circuit.

Measurement on position quadratures

$$\mathbf{y} = \left[\langle \hat{X}_1 \rangle, \langle \hat{X}_2 \rangle, \ldots, \langle \hat{X}_n \rangle \right]. \tag{5}$$

Continuous-Variable quantum neural network

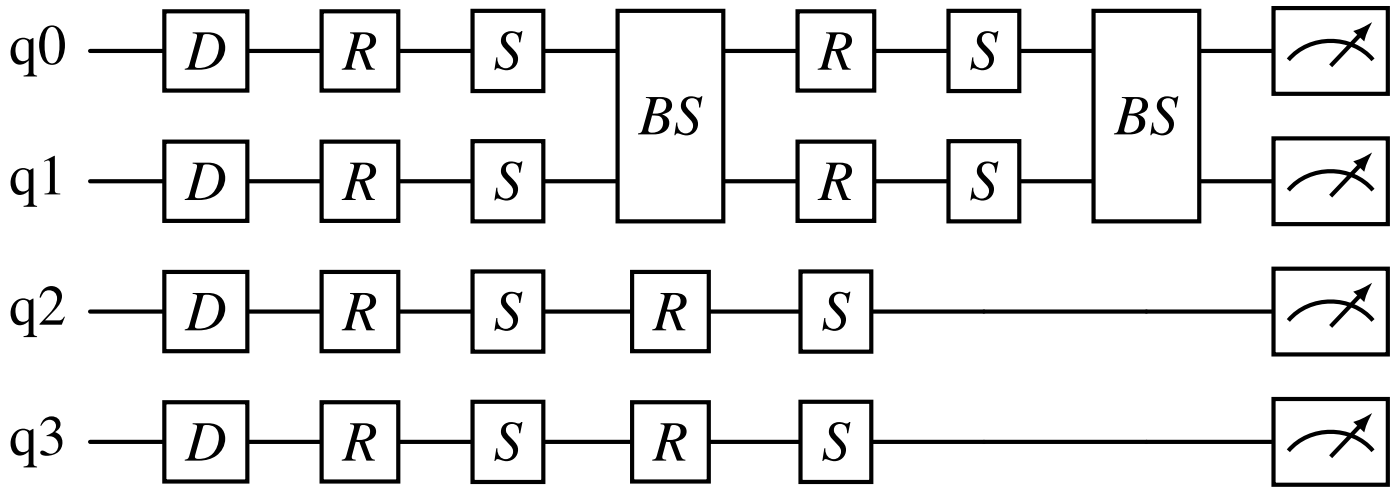

Figure 6: The proposed 4-mode Continuous-Variable (CV) quantum circuit.

Component	**Formula**	**Parameters**	**Description**
Quantum CV Layer	$2 \times 4 \times 4$	32	(D, R, S, BS)
Classical Head	$4 \times 2 + 2$	10	Linear layer mapping
Total	–	**42**	Trainable parameters

Discrete-Variable quantum neural network

Discrete-Variable quantum neural network

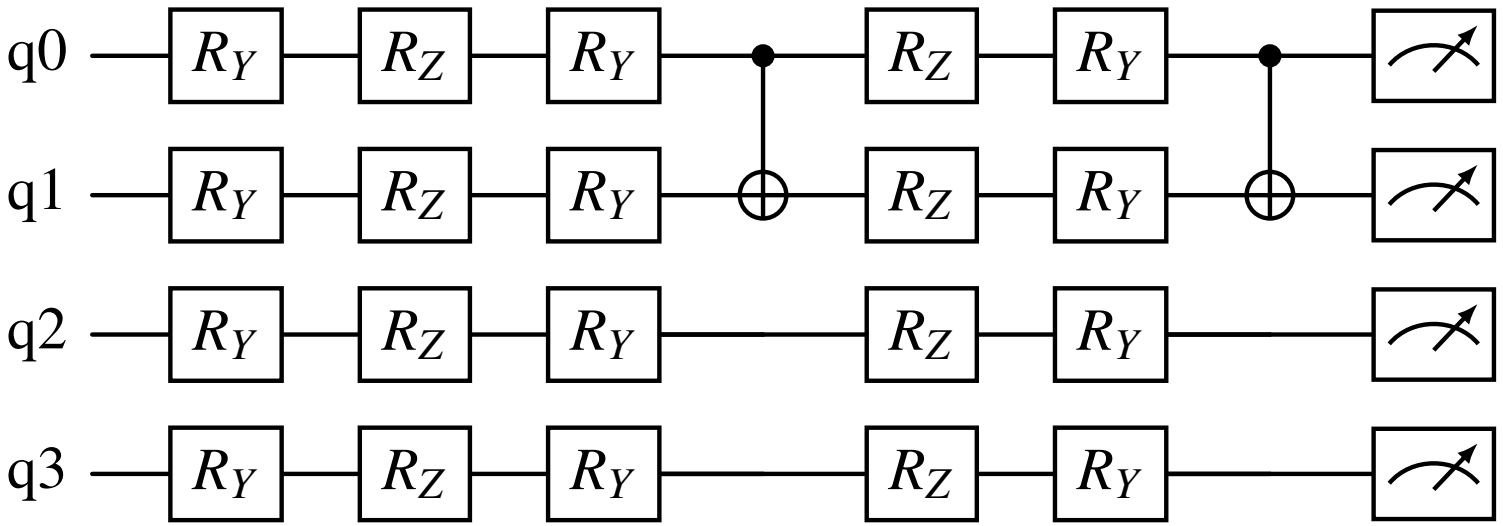

Figure 7: The proposed 4-qubit DV quantum circuit.

Rotation on y-axis gate

$$R_y(\phi) = e^{-i\phi\sigma_y/2} = \begin{bmatrix} \cos(\phi/2) & -\sin(\phi/2) \\ \sin(\phi/2) & \cos(\phi/2) \end{bmatrix}, \tag{6}$$

Discrete-Variable quantum neural network

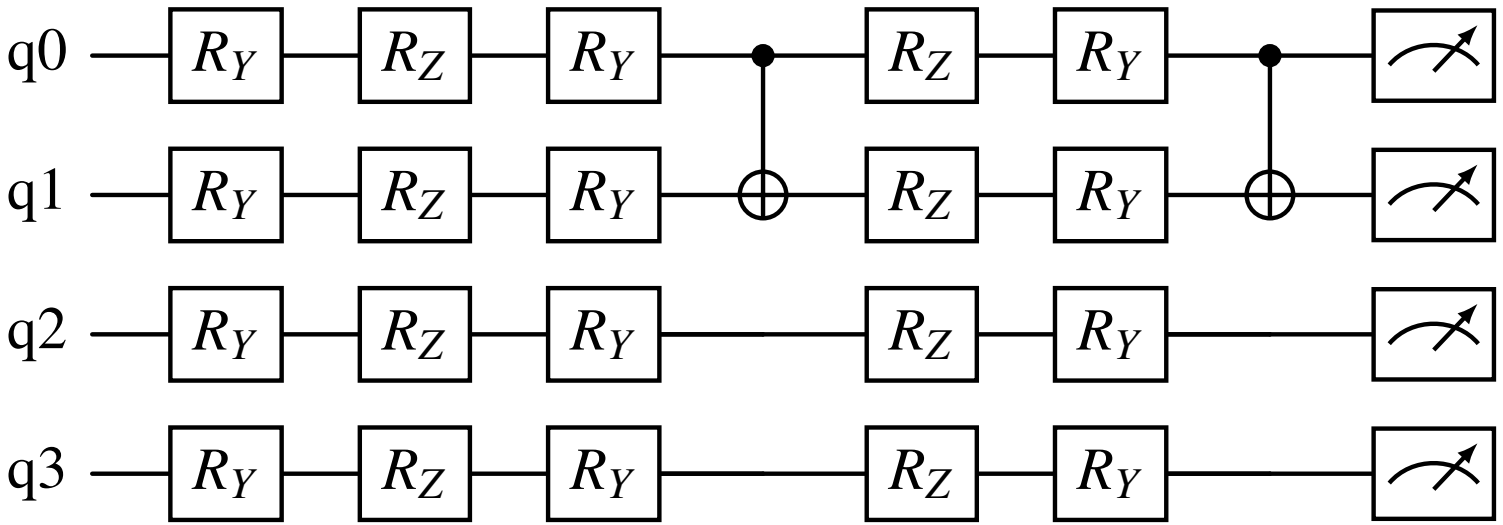

Figure 7: The proposed 4-qubit DV quantum circuit.

Rotation on z-axis gate

$$R_z(\phi) = e^{-i\phi\sigma_z/2} = \begin{bmatrix} e^{-i\phi/2} & 0 \\ 0 & e^{i\phi/2} \end{bmatrix}. \tag{7}$$

Discrete-Variable quantum neural network

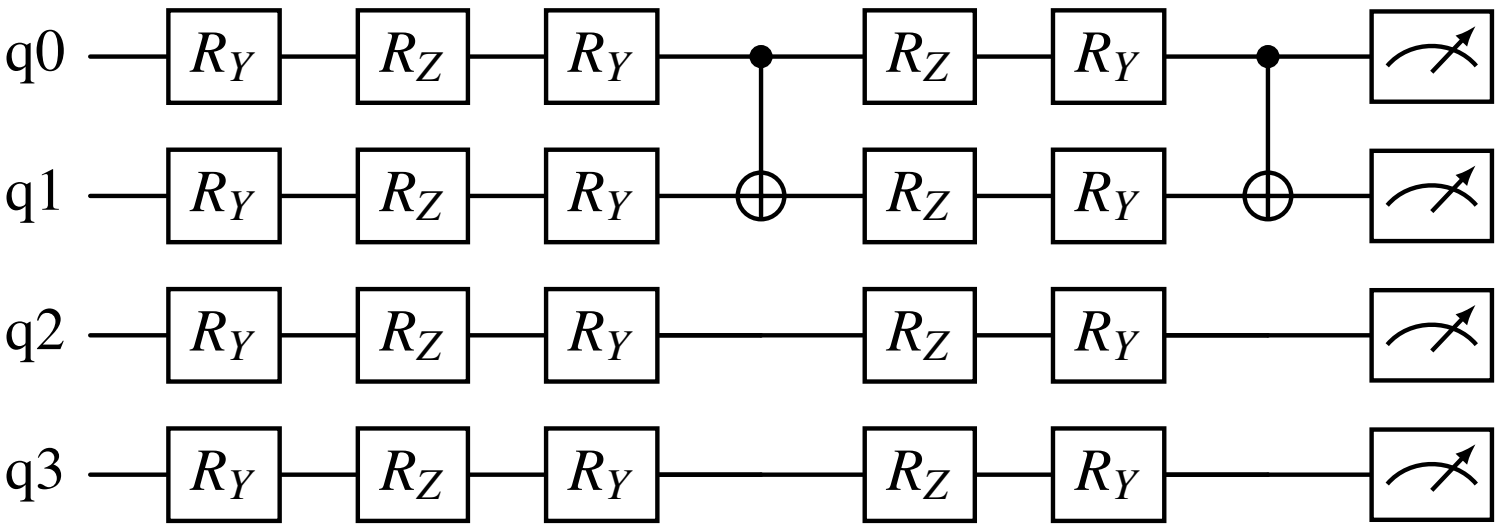

Figure 7: The proposed 4-qubit DV quantum circuit.

Controlled NOT gate

$$\text{CNOT} = |0\rangle\langle 0| \otimes I + |1\rangle\langle 1| \otimes X = \begin{bmatrix} 1 & 0 & 0 & 0 \\ 0 & 1 & 0 & 0 \\ 0 & 0 & 0 & 1 \\ 0 & 0 & 1 & 0 \end{bmatrix}. \tag{8}$$

Discrete-Variable quantum neural network

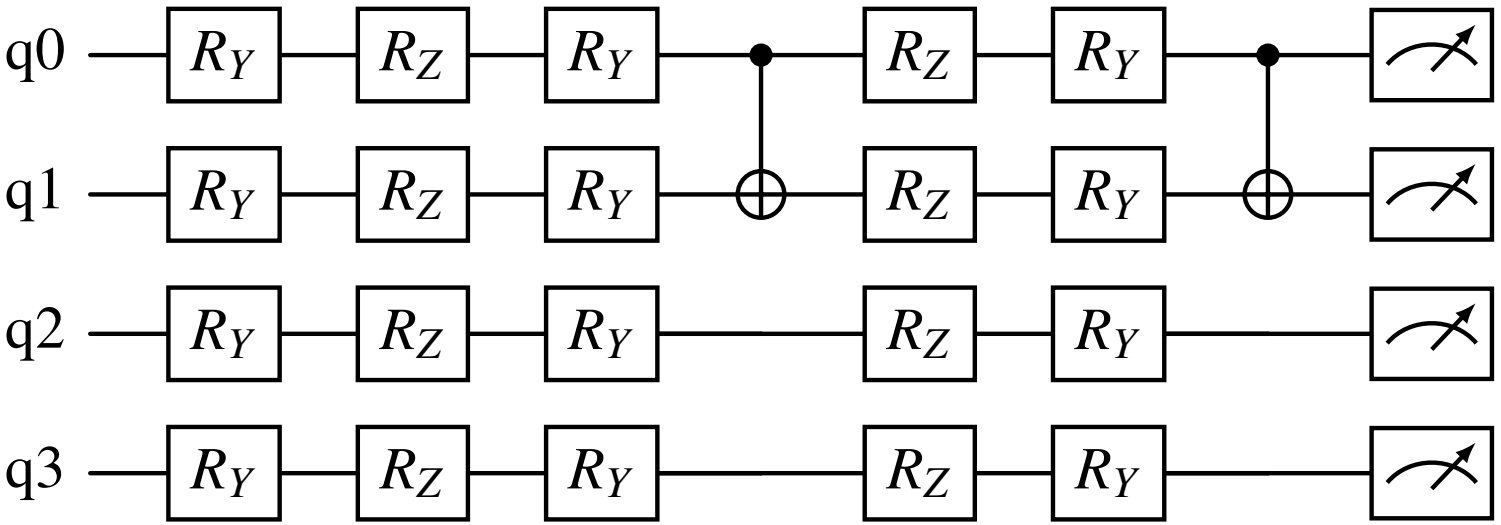

Figure 7: The proposed 4-qubit DV quantum circuit.

Measurement along the z-axis

$$\text{Measurement} = \langle\psi|\sigma_z|\psi\rangle, \tag{9}$$

Discrete-Variable quantum neural network

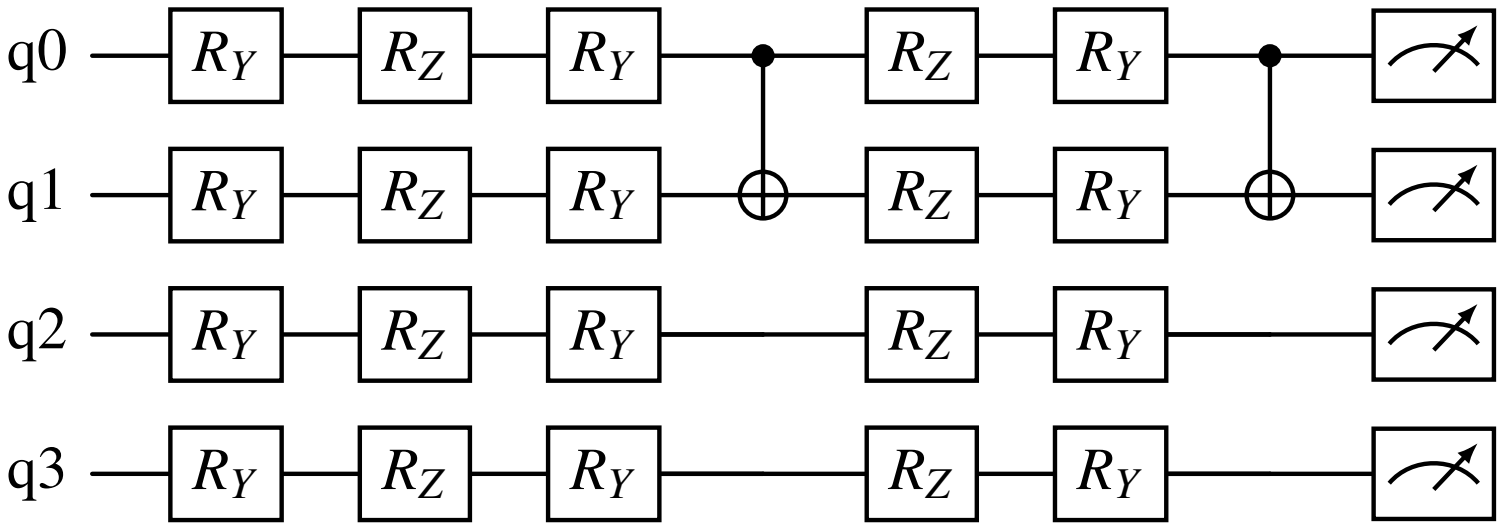

Figure 7: The proposed 4-qubit DV quantum circuit.

Component	**Formula**	**Parameters**	**Description**
Quantum DV Layer	$2 \times 4 \times 4$	32	(R_Y, R_Z, R_Y, R_Z)
Classical Head	$4 \times 2 + 2$	10	Linear layer mapping
Total	–	**42**	Trainable parameters

Classification Metrics and Confusion Matrix

Classification Metrics

$$P = \frac{TP}{TP + FP},$$

$$R = \frac{TP}{TP + FN},$$

$$ACC = \frac{TP + TN}{TP + TN + FP + FN},$$

$$F1 = 2\left(\frac{P \times R}{P + R}\right). \qquad (10)$$

P: Precision,
R: Recall,
ACC: Accuracy,
F1: F1-score.

Confusion Matrix (Class B)

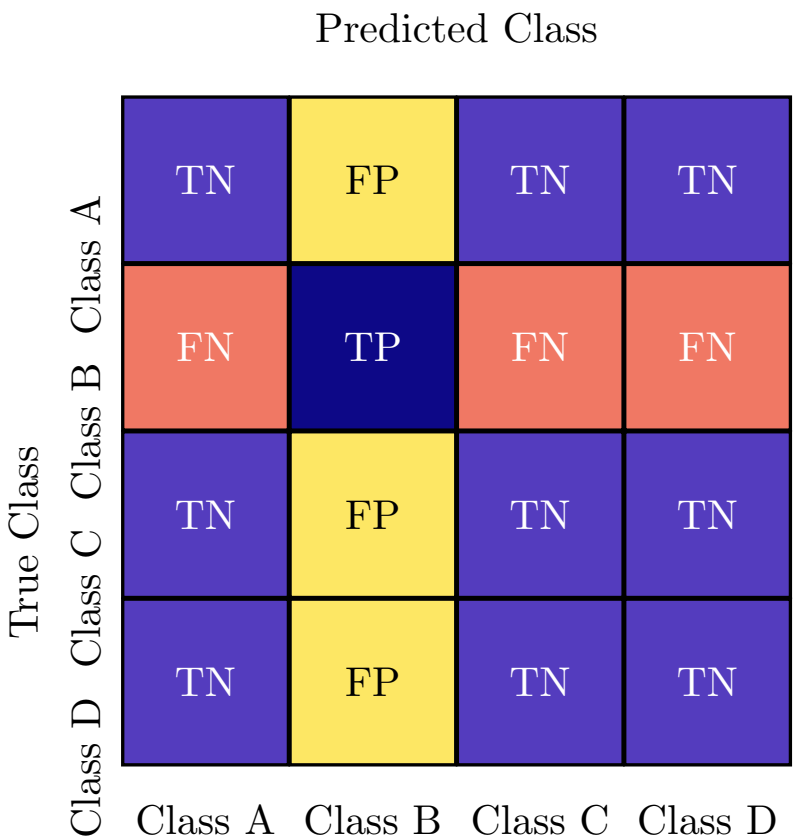

Figure 8: Multiclass confusion matrix for class B.

Area under the characteristic operating curve

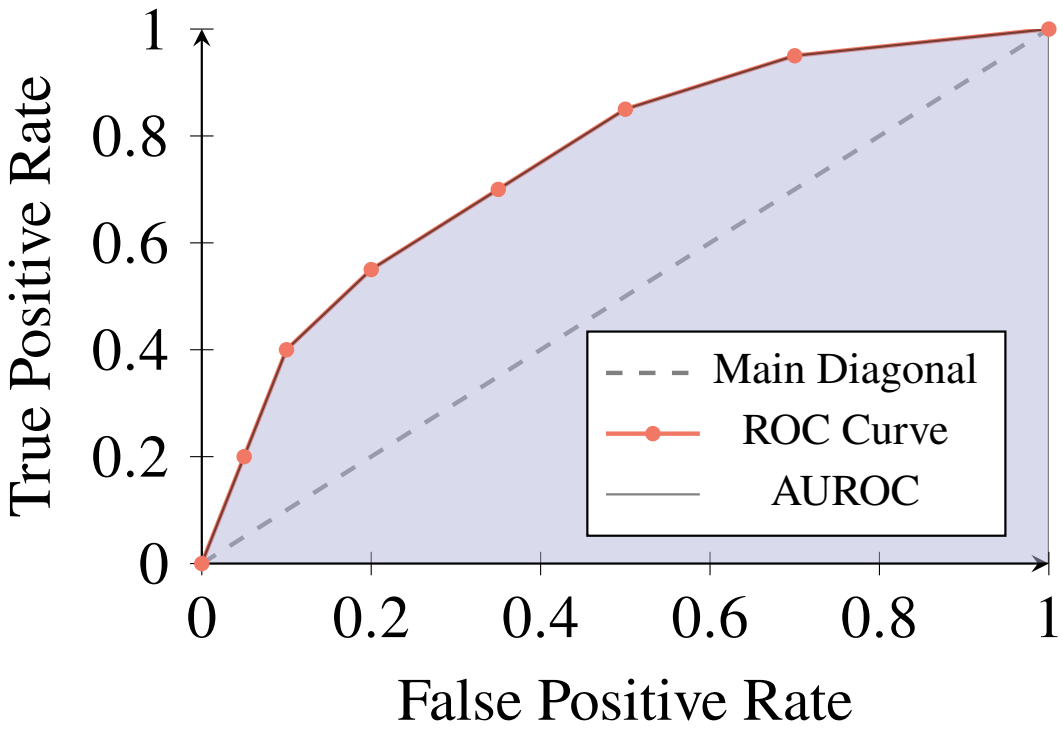

Figure 9: Area under Receiver Operating Characteristic (ROC) curve.

$$AUROC(\sigma) = \int_a^b TPR(\sigma) d(FPR(\sigma). \tag{11}$$

4.- Experiments and results

Classification performance on PneumoniaMNIST

Classification performance on PneumoniaMNIST

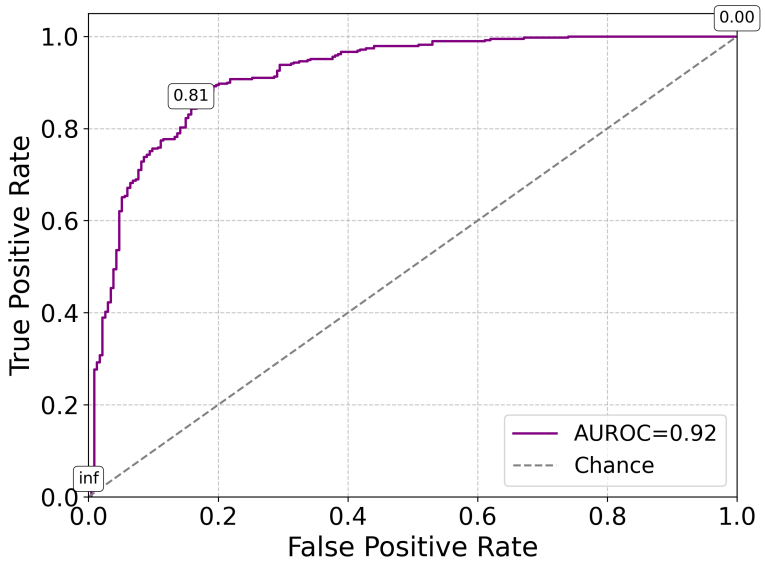

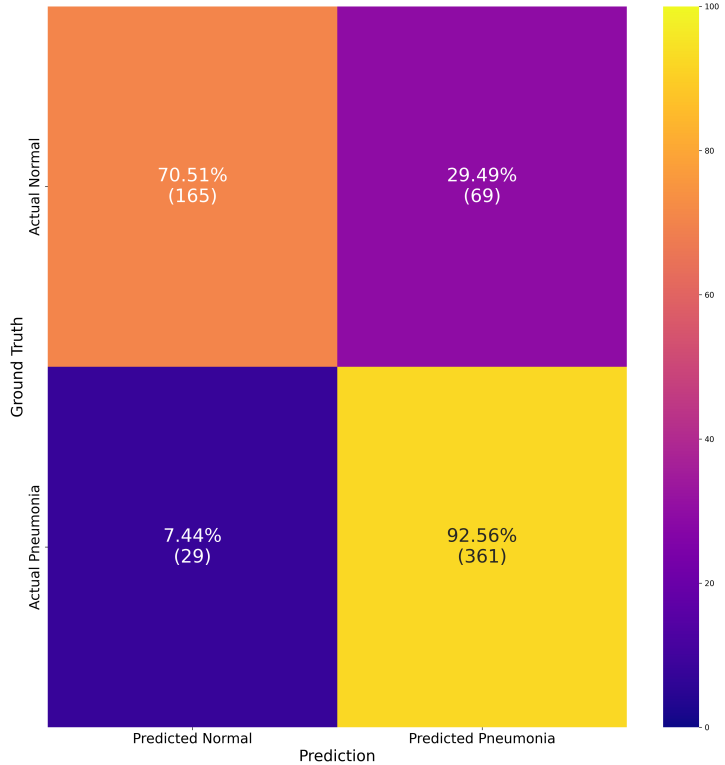

Figure 10: Results for CV QNN on PneumoniaMNIST dataset.

Classification performance on PneumoniaMNIST

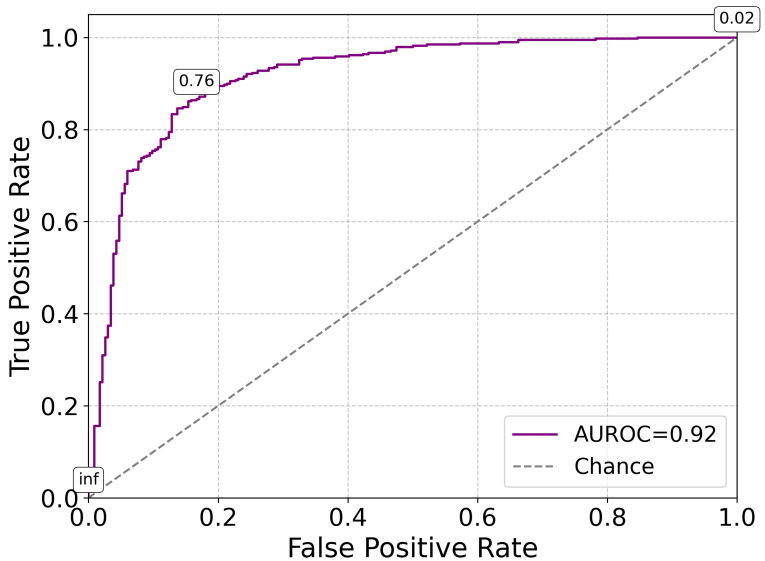

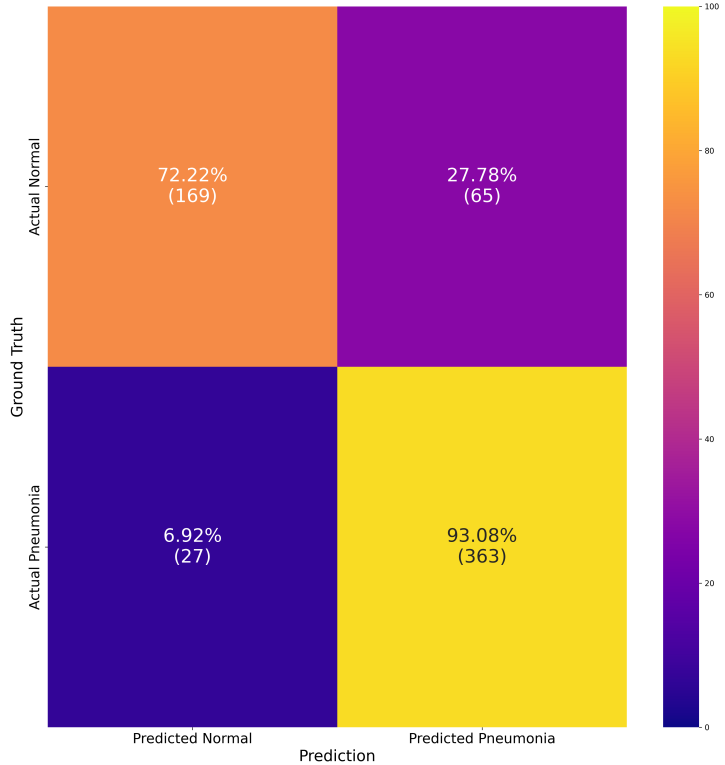

Figure 11: Results for DV QNN on PneumoniaMNIST dataset.

Classification performance on PneumoniaMNIST

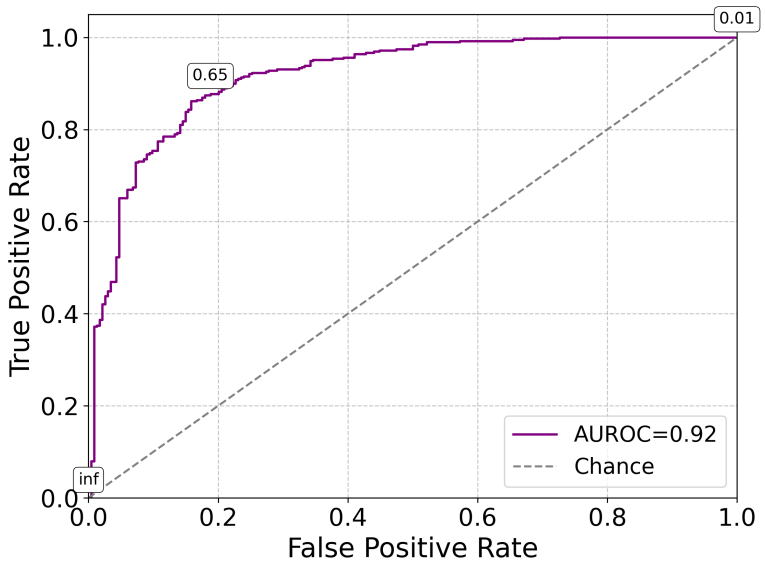

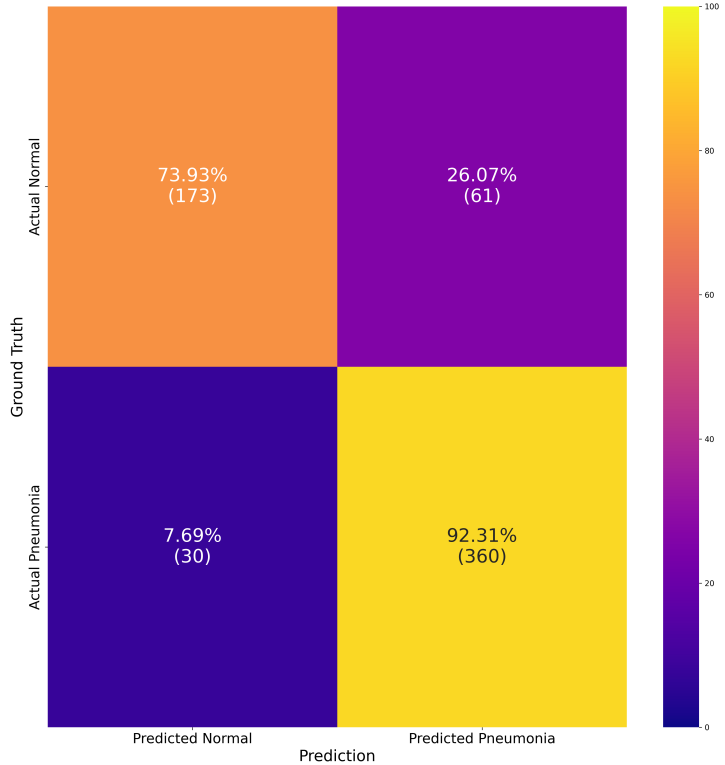

Figure 12: Results for classical NN on PneumoniaMNIST dataset.

Classification performance on OrganAMNIST

Classification performance on OrganAMNIST

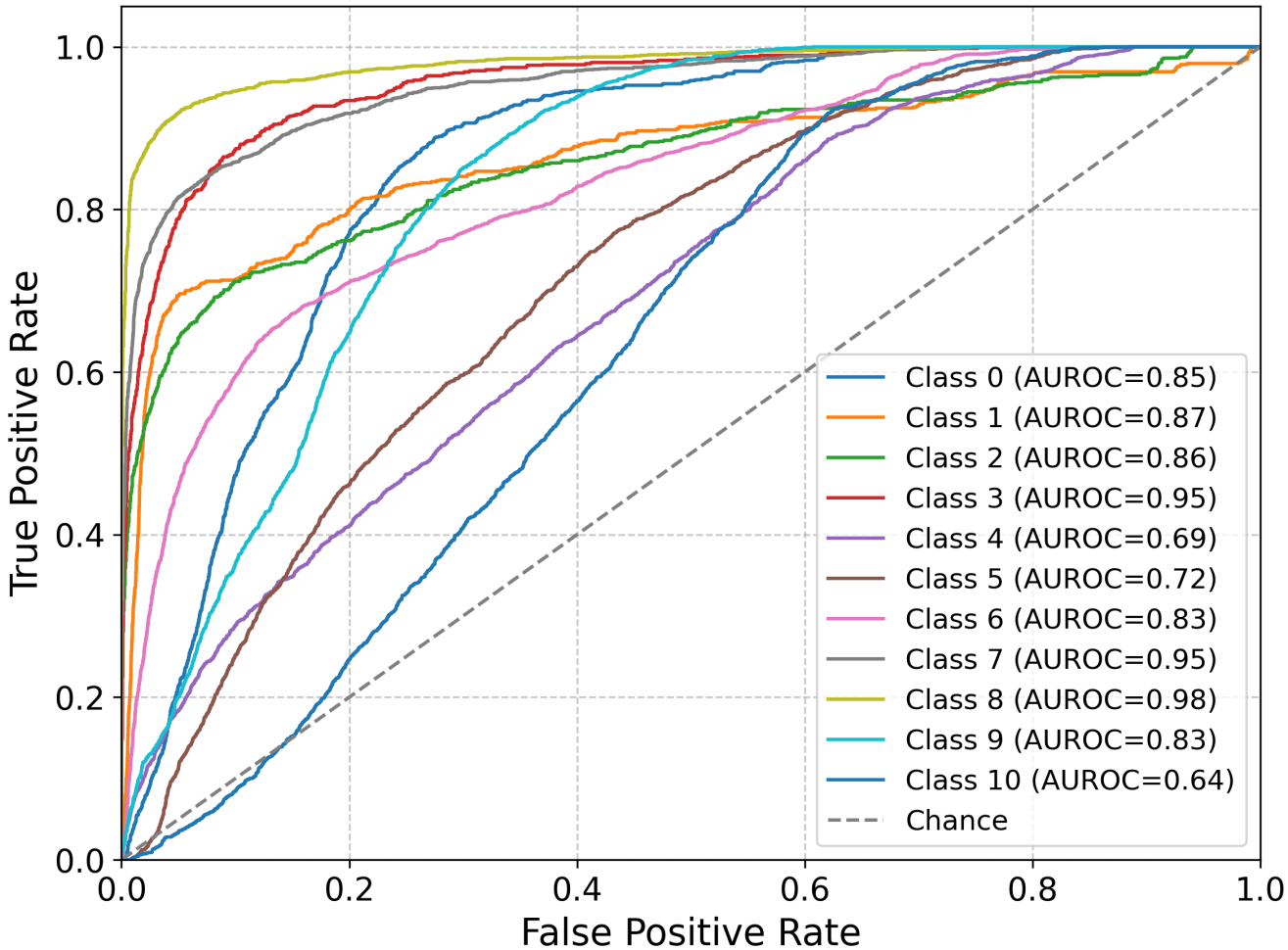

Figure 13: AUROC of CV QNN for OrganAMNIST dataset.

Classification performance on OrganAMNIST

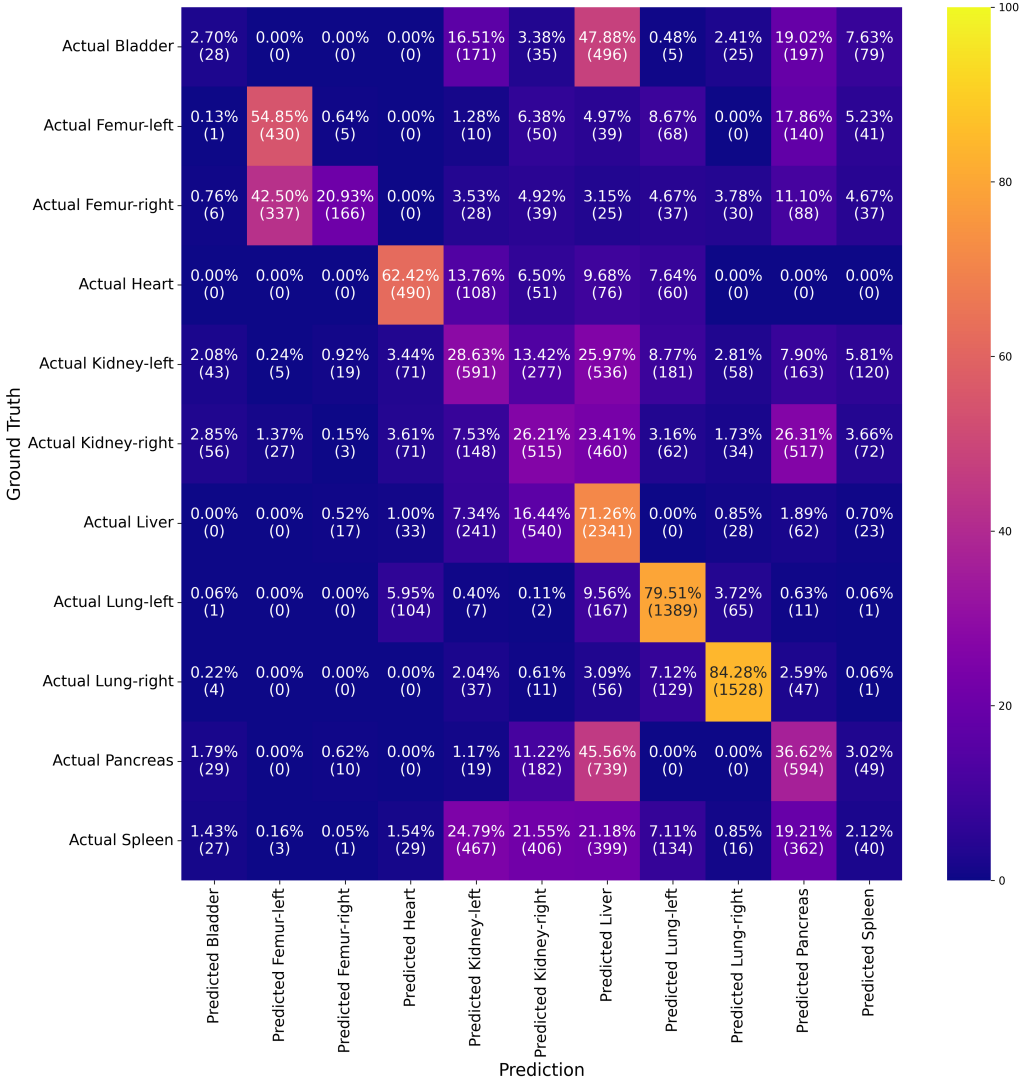

Figure 14: Confusion matrix of CV QNN for OrganAMNIST dataset.

Classification performance on OrganAMNIST

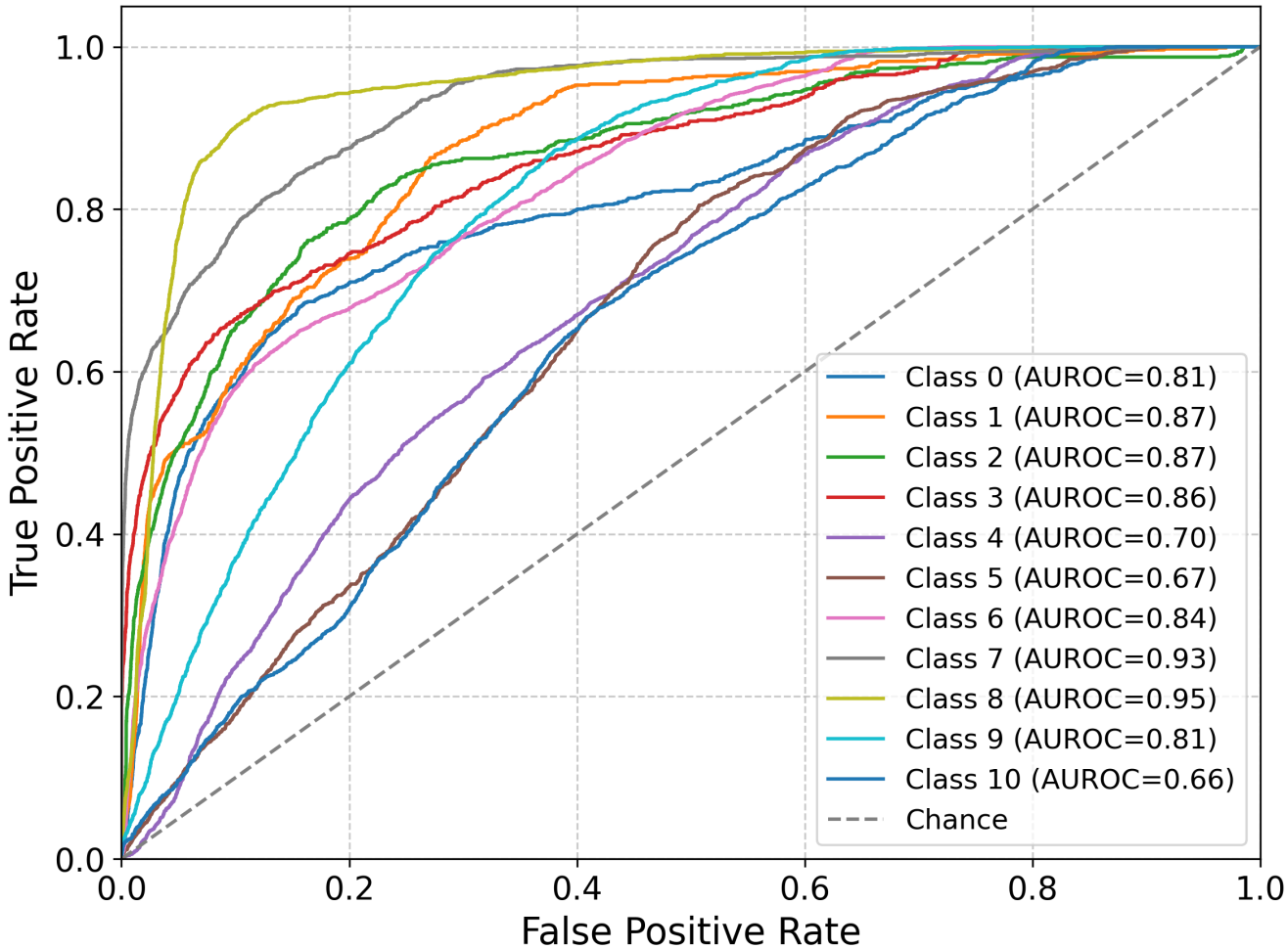

Figure 15: AUROC of DV QNN for OrganAMNIST dataset.

Classification performance on OrganAMNIST

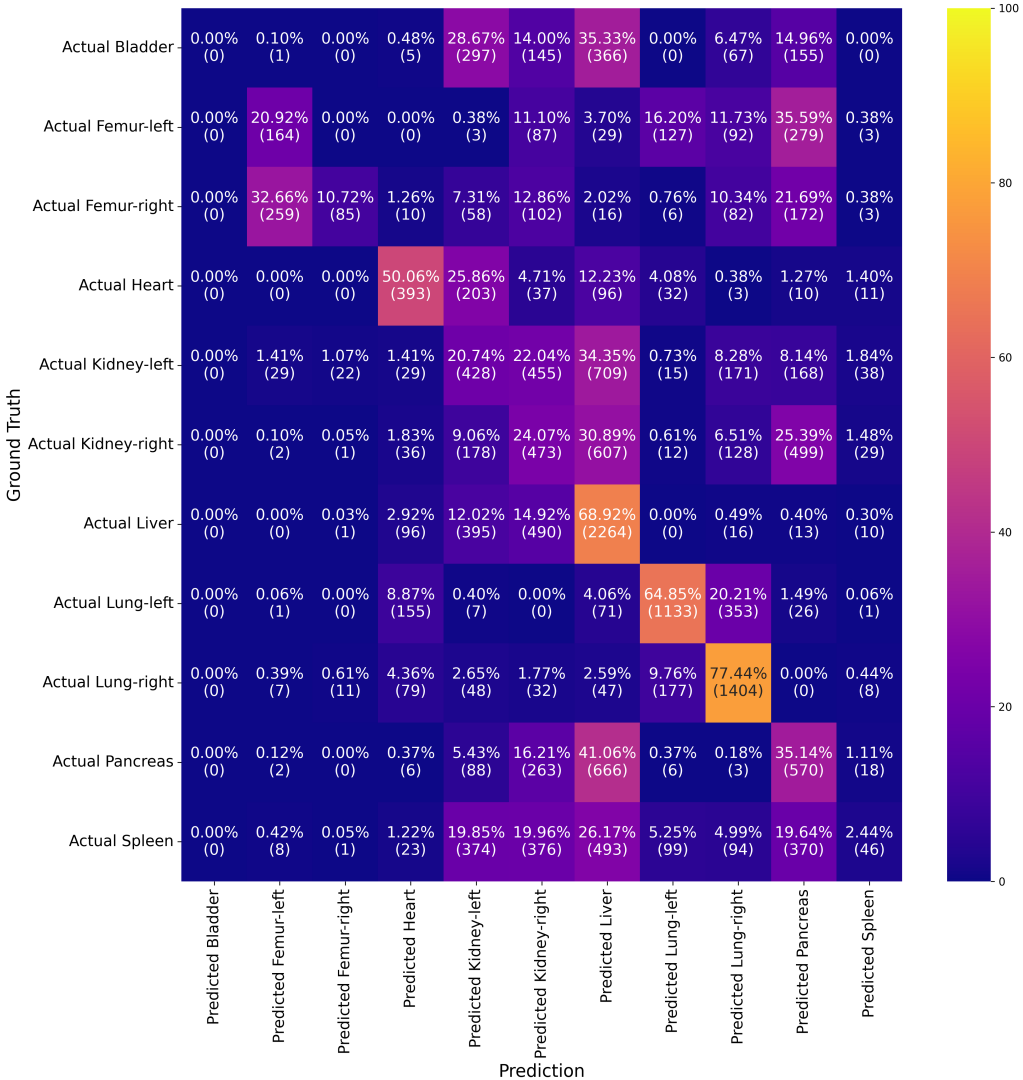

Figure 16: Confusion matrix of DV QNN for OrganAMNIST dataset.

Classification performance on OrganAMNIST

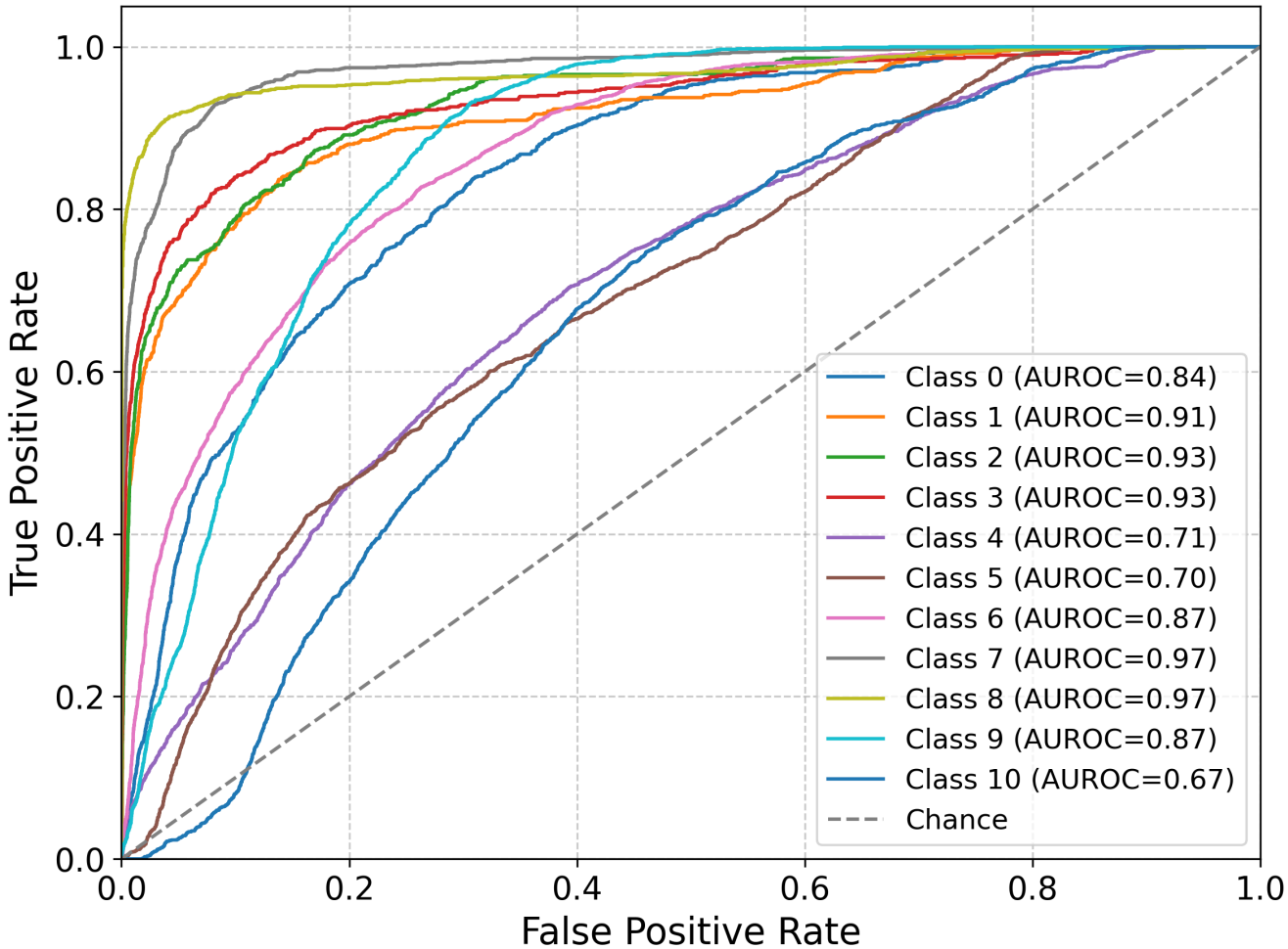

Figure 17: AUROC of classical NN for OrganAMNIST dataset.

Classification performance on OrganAMNIST

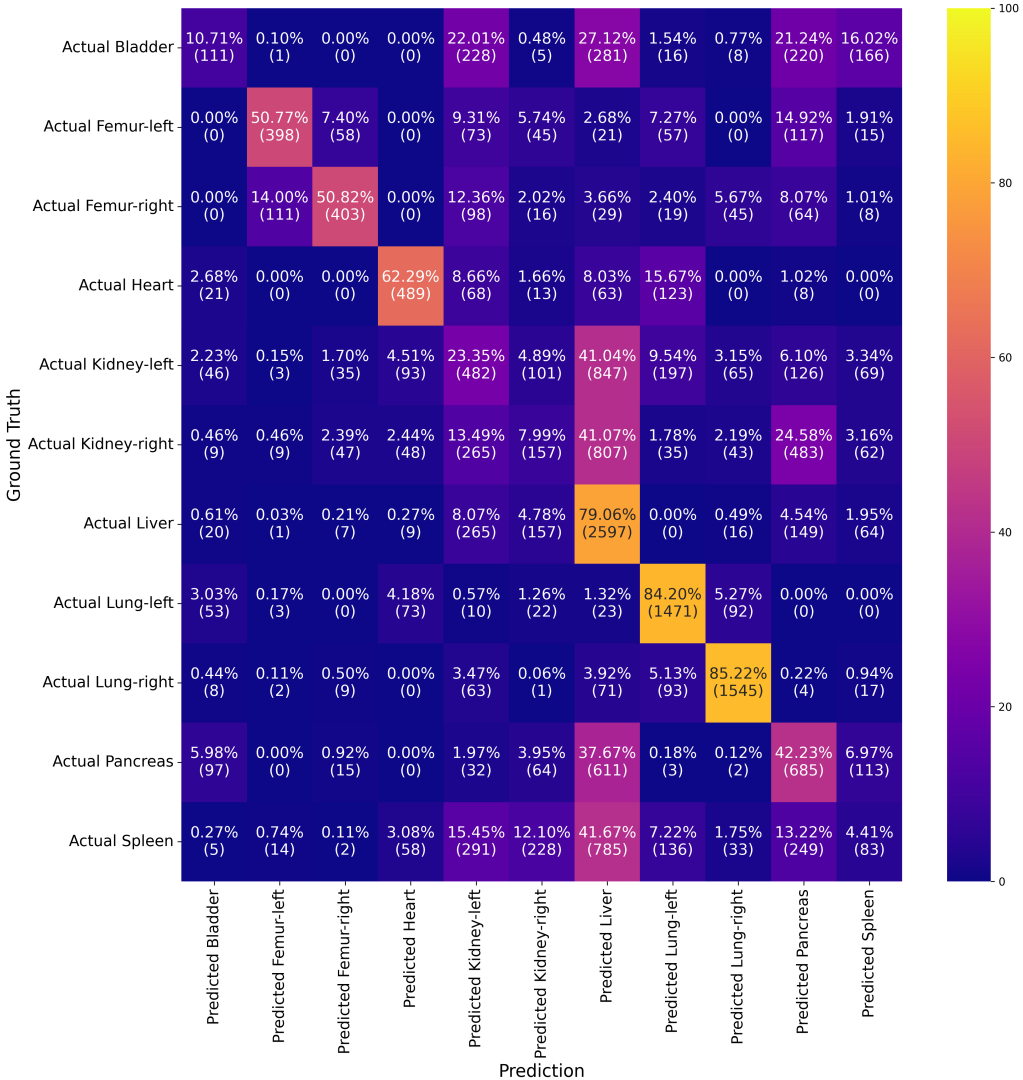

Figure 18: Confusion matrix of classical NN for OrganAMNIST dataset.

Classification performance on BreastMNIST

Classification performance on BreastMNIST

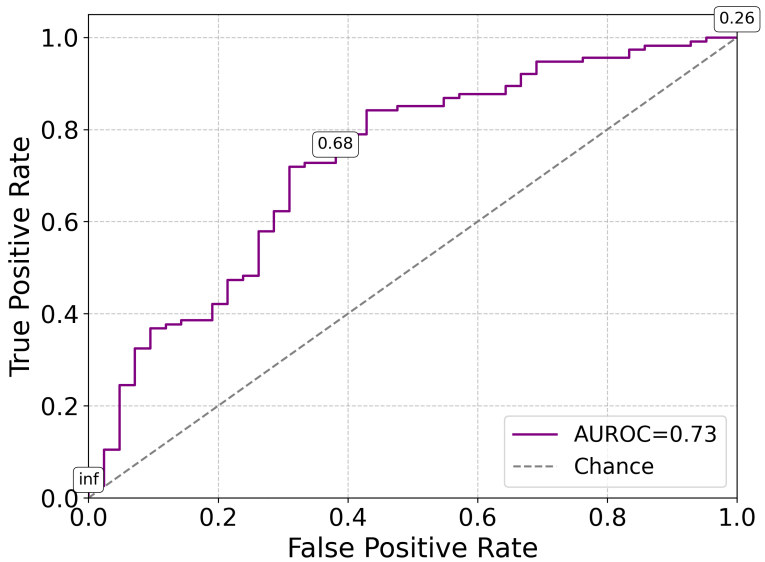

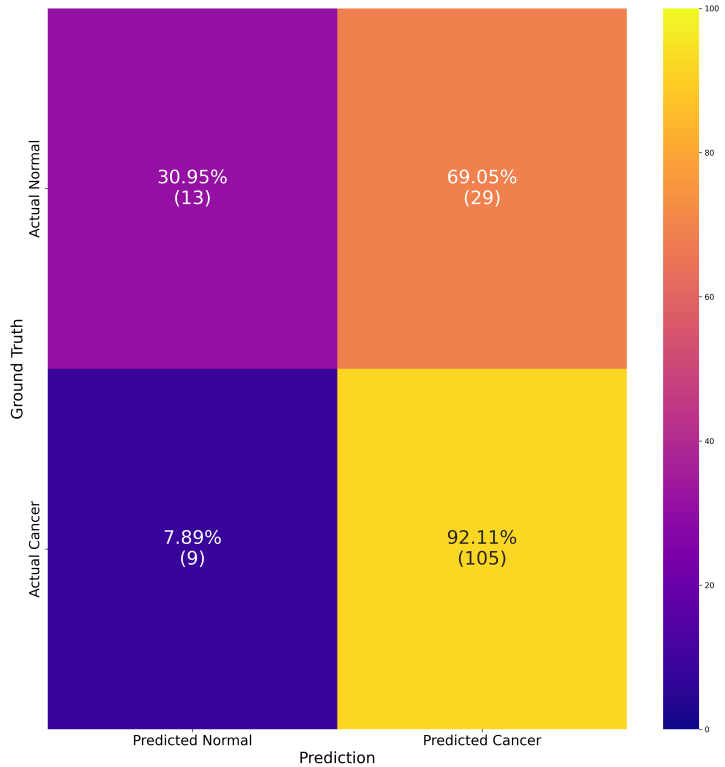

Figure 19: Results for CV QNN on BreastMNIST dataset.

Classification performance on BreastMNIST

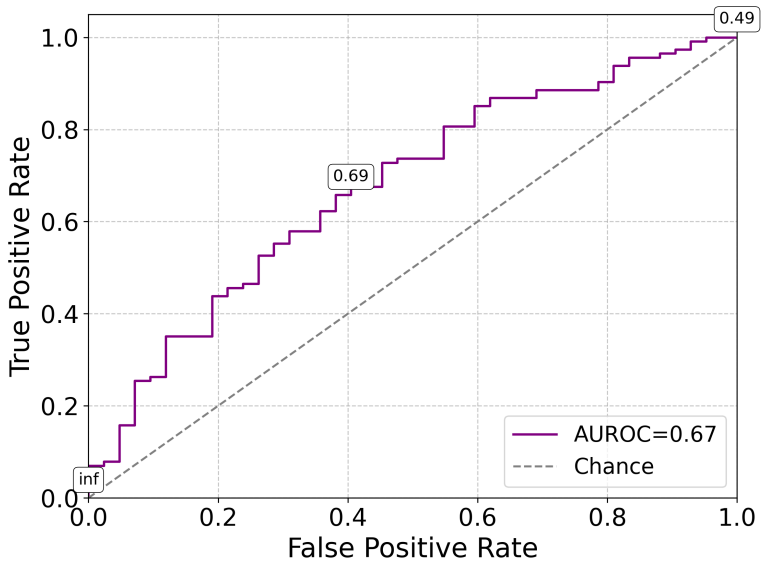

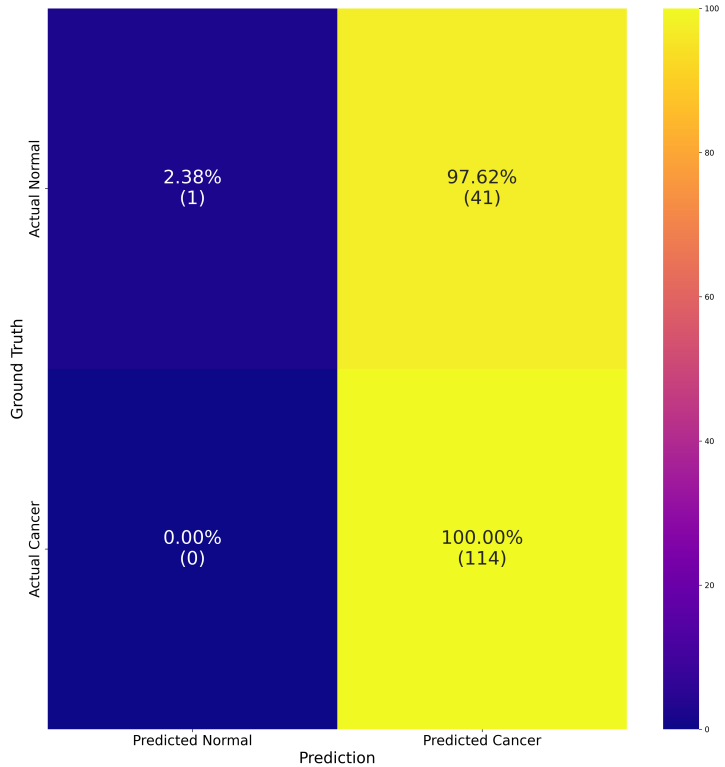

Figure 20: Results for DV QNN on BreastMNIST dataset.

Classification performance on BreastMNIST

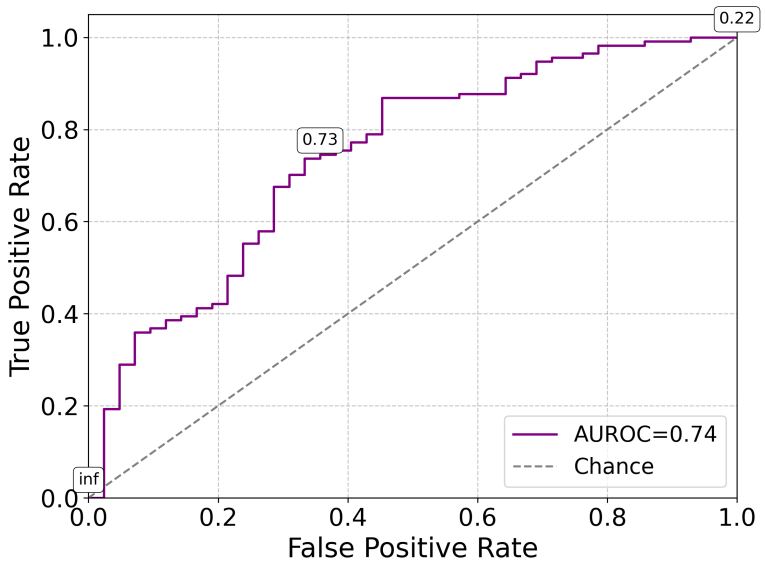

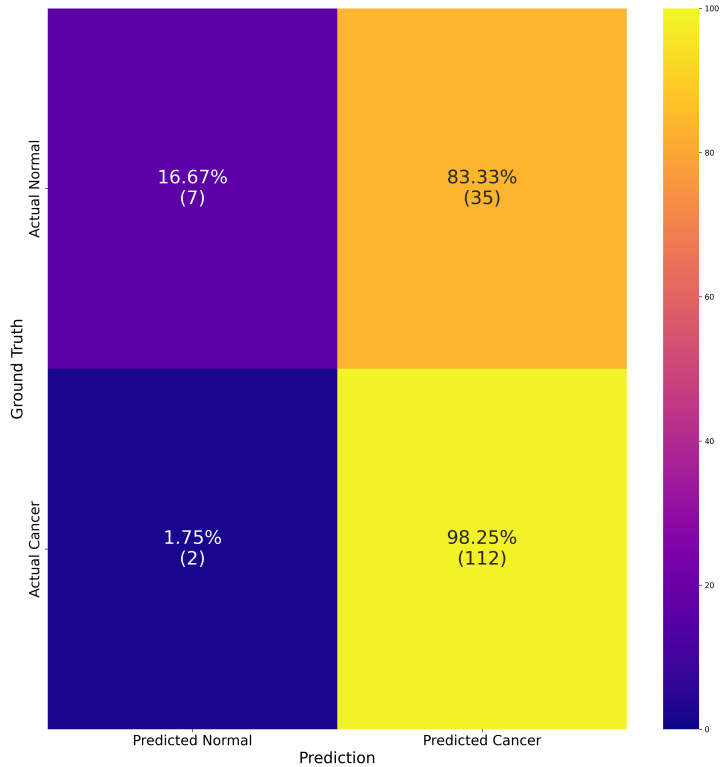

Figure 21: Results for classical NN on BreastMNIST dataset.

Gaussian noise robustness comparison

Gaussian noise robustness comparison

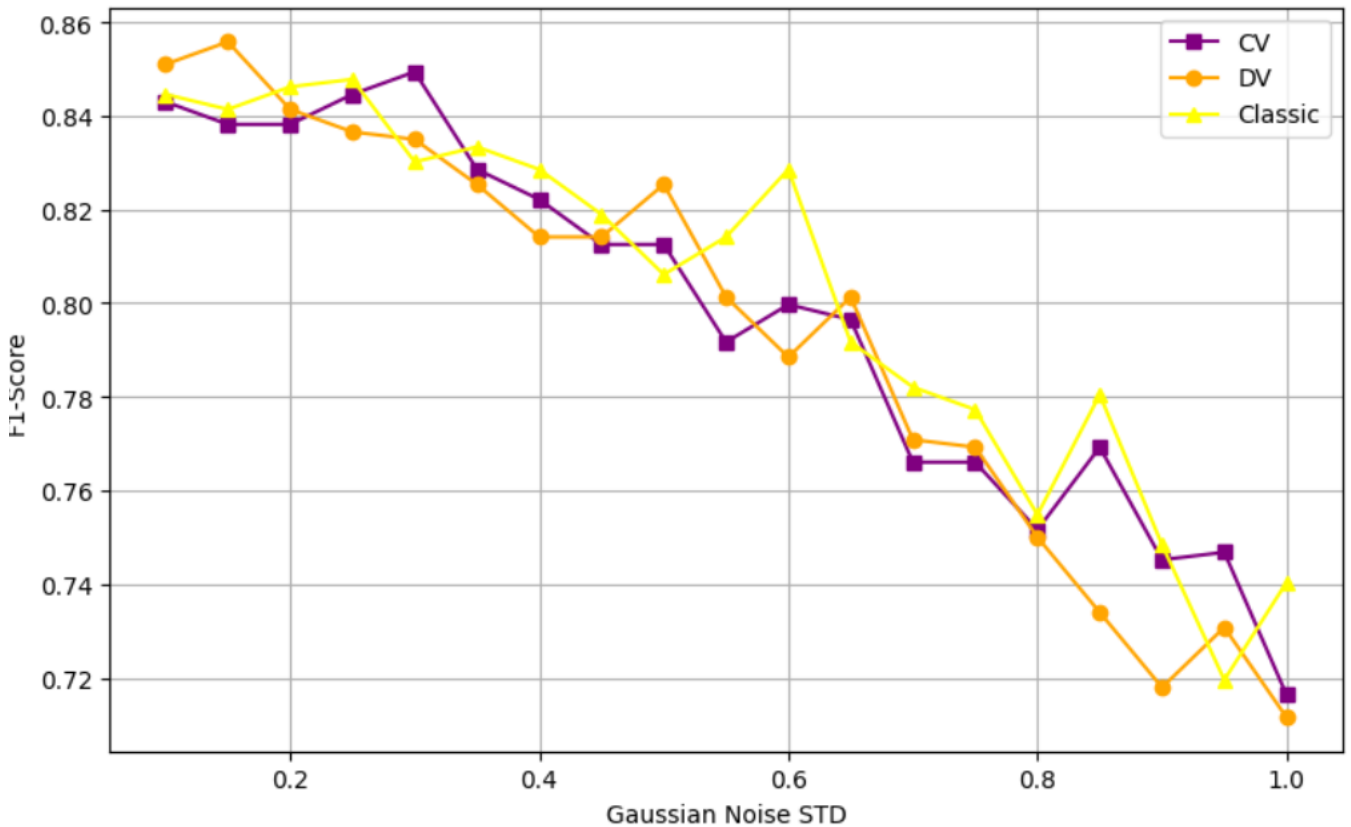

Figure 22: F1 score comparison on Gaussian noise for PneumoniaMNIST dataset.

Gaussian noise robustness comparison

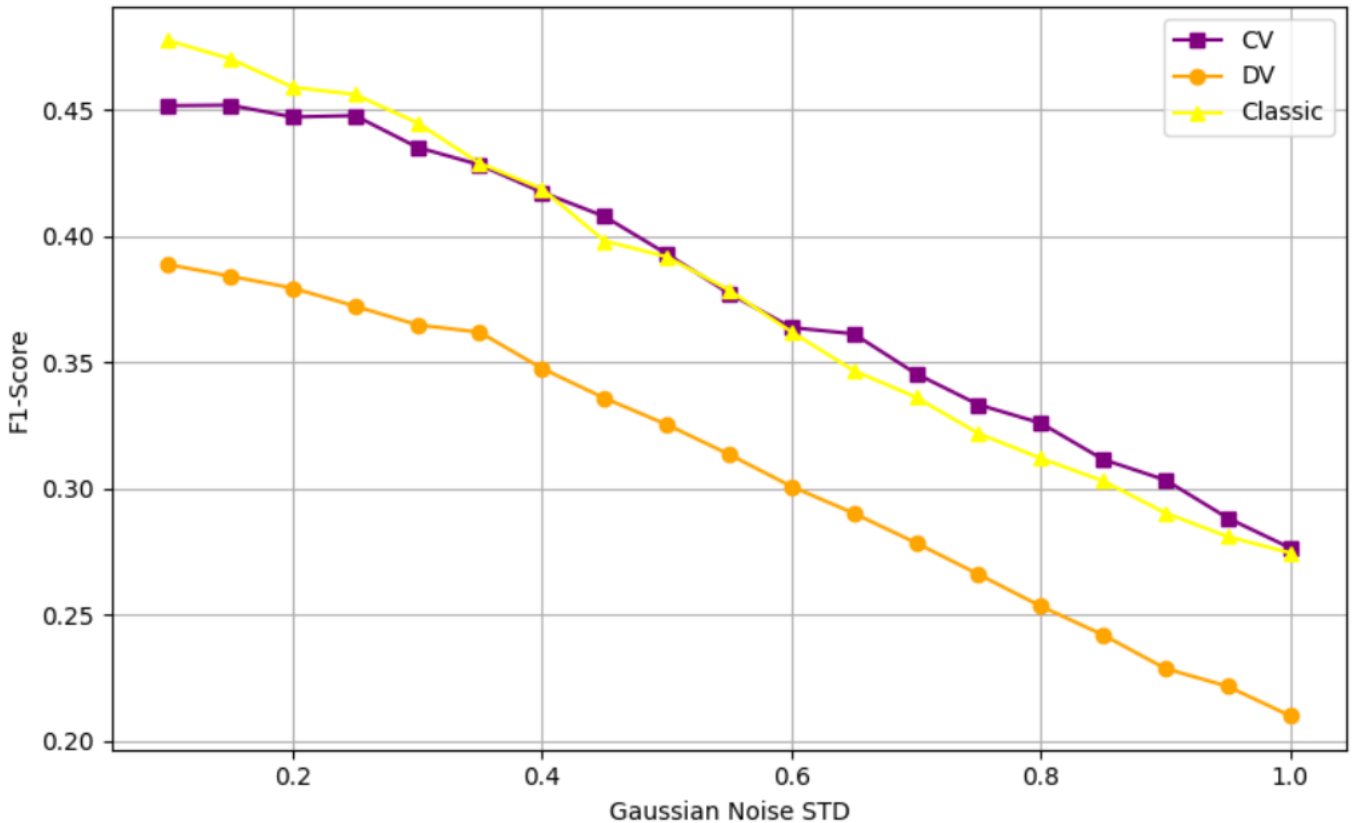

Figure 23: F1 score comparison on Gaussian noise for for OrganAMNIST dataset.

Gaussian noise robustness comparison

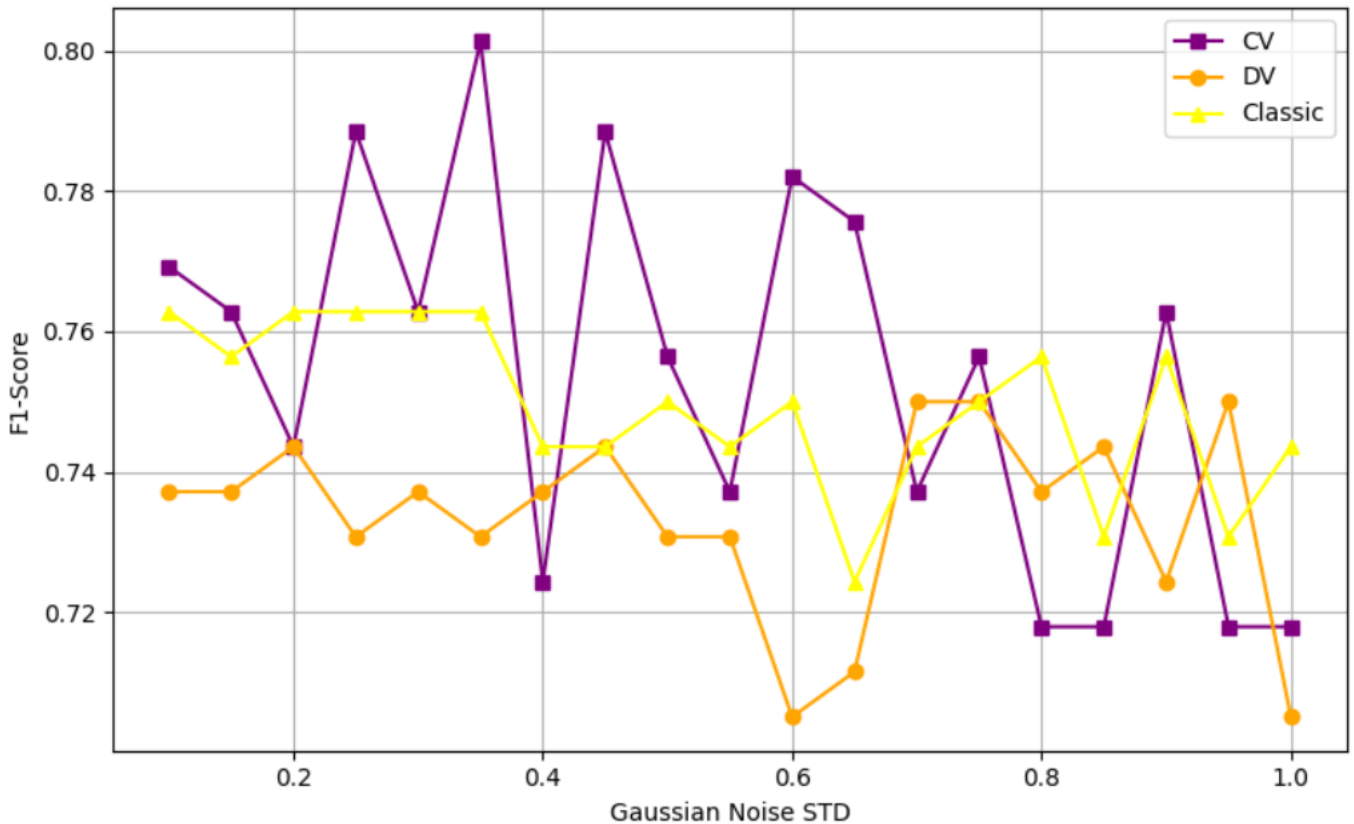

Figure 24: F1 score comparison on Gaussian noise for BreastMNIST.

Test set results summary

Table 2: Test set classification metrics.

Model	Dataset	ACC	P	R	F1	AUROC	AUPRC
CV QNN	BreastMNIST	0.7564	0.7564	0.7317	0.7564	0.73	**0.86**
	OrganAMNIST	0.4563	0.4563	0.4257	0.4563	0.8333	0.4554
	PneumoniaMNIST	0.8429	0.8429	0.8437	0.8429	**0.92**	**0.93**
DV QNN	BreastMNIST	0.7372	0.7372	0.7662	0.7372	0.67	0.84
	OrganAMNIST	0.3915	0.3915	0.3714	0.3915	0.8154	0.3754
	PneumoniaMNIST	**0.8542**	**0.8542**	0.8534	0.8526	**0.92**	**0.93**
Classical	BreastMNIST	**0.7628**	**0.7628**	**0.7662**	**0.7628**	**0.74**	**0.86**
	OrganAMNIST	**0.4737**	**0.4737**	**0.4355**	**0.4737**	**0.8518**	**0.49**
	PneumoniaMNIST	**0.8542**	**0.8542**	**0.8540**	**0.8542**	**0.92**	**0.93**

Decision heatmap comparison

Decision heatmap comparison

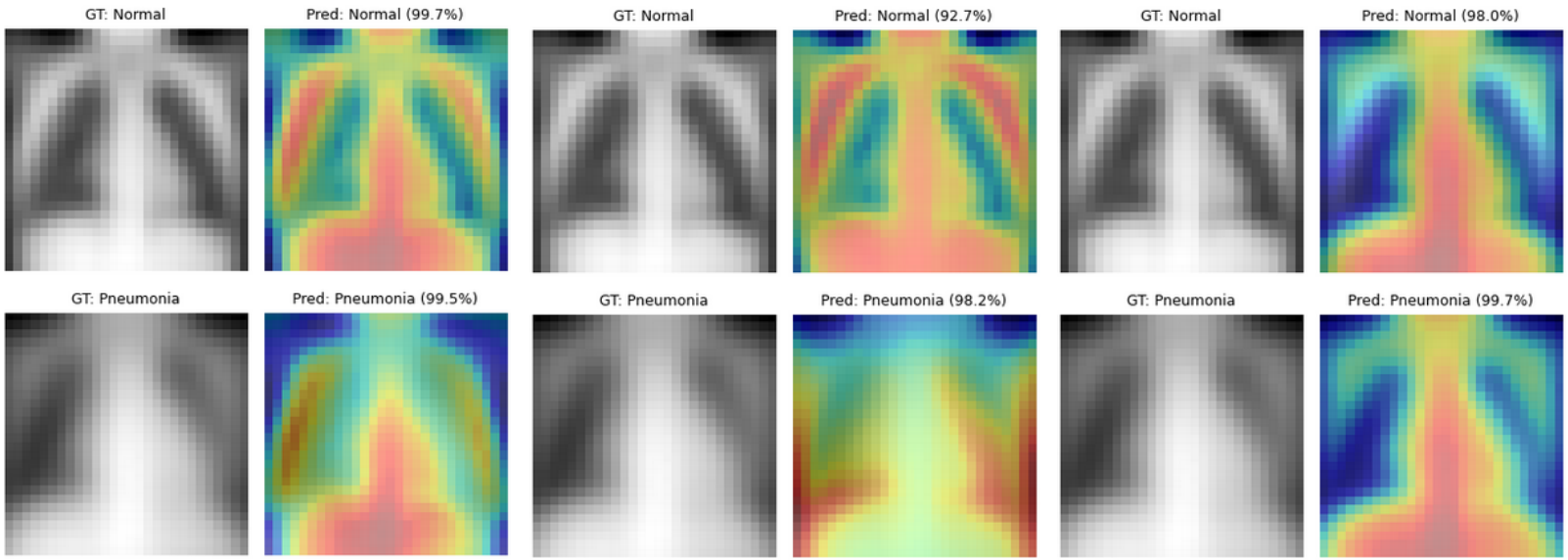

Figure 25: Decision heatmap GradCAM comparison on PneumoniaMNIST.

Decision heatmap comparison

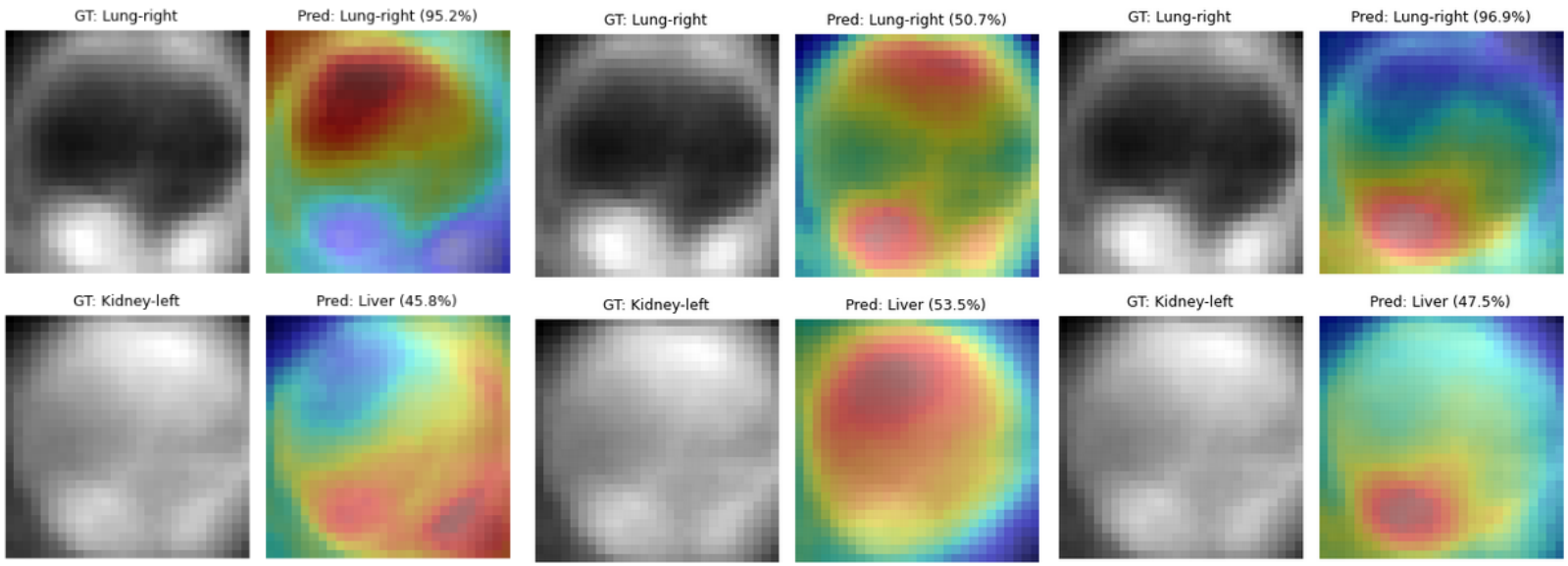

Figure 26: Decision heatmap GradCAM comparison on OrganAMNIST.

Decision heatmap comparison

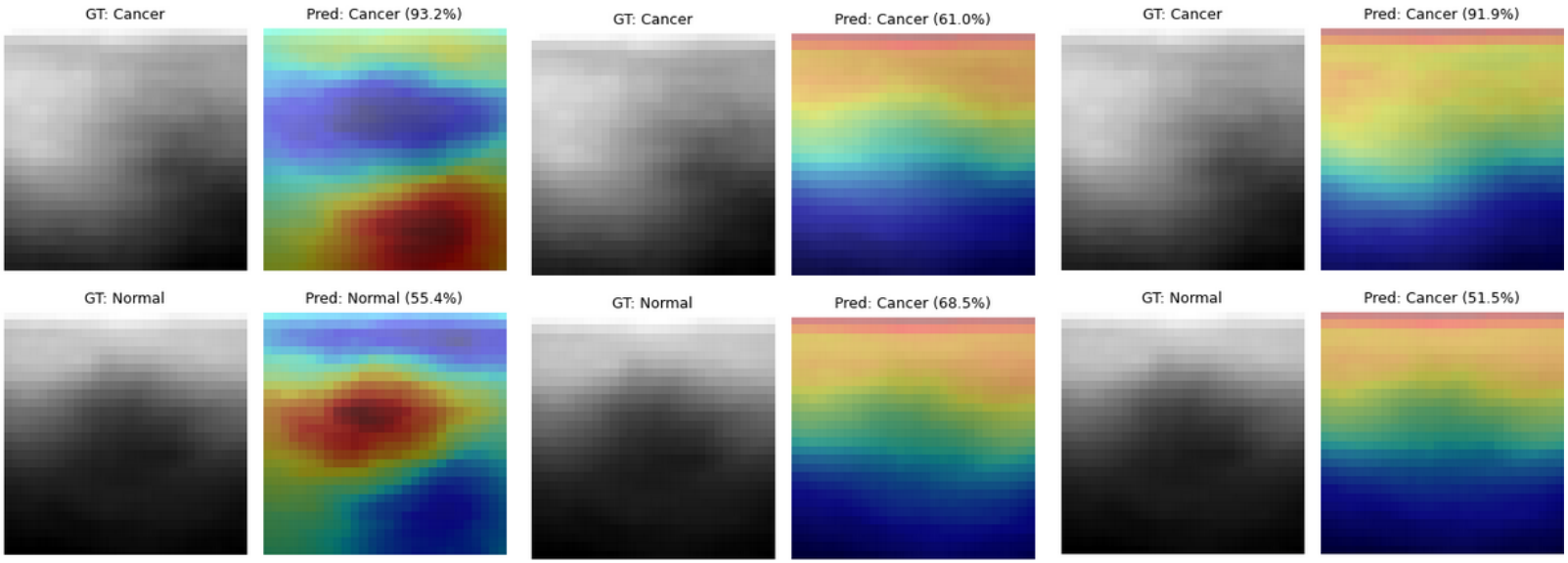

CV QNN DV QNN Classical

Figure 27: Decision heatmap GradCAM comparison.

5.- Conclusions and future work

Conclusions

Conclusions

- The proposed CV and DV quantum models attain **comparable classification performance** to their classical counterpart (F1 scores of 75% in BreastMNIST, 45% OrganAMNIST, 85% in PneumoniaMNIST).

Conclusions

- The proposed CV and DV quantum models attain **comparable classification performance** to their classical counterpart (F1 scores of 75% in BreastMNIST, 45% OrganAMNIST, 85% in PneumoniaMNIST).
- The proposed CV QNN shows slightly **higher performance** than its DV quantum counterpart in **multiclass classification** (+7% F1 score in OrganMNIST), and **slight advantage on minority class** focus (15% TN samples of BreastMNIST).

Conclusions

- The proposed CV and DV quantum models attain **comparable classification performance** to their classical counterpart (F1 scores of 75% in BreastMNIST, 45% OrganAMNIST, 85% in PneumoniaMNIST).
- The proposed CV QNN shows slightly **higher performance** than its DV quantum counterpart in **multiclass classification** (+7% F1 score in OrganMNIST), and **slight advantage on minority class** focus (15% TN samples of BreastMNIST).
- Noise robustness testing shows **high resilience** for the CV QNN, demonstrating stability close to its classical counterpart over different levels of Gaussian noise.

Conclusions

- The proposed CV and DV quantum models attain **comparable classification performance** to their classical counterpart (F1 scores of 75% in BreastMNIST, 45% OrganAMNIST, 85% in PneumoniaMNIST).
- The proposed CV QNN shows slightly **higher performance** than its DV quantum counterpart in **multiclass classification** (+7% F1 score in OrganMNIST), and **slight advantage on minority class** focus (15% TN samples of BreastMNIST).
- Noise robustness testing shows **high resilience** for the CV QNN, demonstrating stability close to its classical counterpart over different levels of Gaussian noise.
- Decision heatmaps of the proposed CV QNN shows **more interpretable highlighted areas**, particularly on the BreastMNIST dataset.

Future work

Future work

- Additional data preparation processes to **maximize data feature representation**.

Future work

- Additional data preparation processes to **maximize data feature representation**.
- Test the proposed quantum models on **more complex datasets**.

Future work

- Additional data preparation processes to **maximize data feature representation**.
- Test the proposed quantum models on **more complex datasets**.
- Further **development on quantum circuit** depth, qumode count, trainable parameters, as well as the introduction of non Gaussian gates.

Acknowledgements

Collaborators

Dr. Oscar Montiel

CITEDI – IPN

Dr. Miguel Angel Lopez

CETYS Universidad

Dr. Oscar Castillo

Instituto Tecnológico de Tijuana

Presentation references

[1] Andre Esteva et al. 'Dermatologist-level classification of skin cancer with deep neural networks'. In: *Nature* 542 (7639 Feb. 2017), pp. 115–118. ISSN: 1476-4687. DOI: 10.1038/NATURE21056

[2] Constanze Polzer et al. 'AI-based automated detection and stability analysis of traumatic vertebral body fractures on computed tomography'. In: *European Journal of Radiology* 173 (Apr. 2024). ISSN: 18727727. DOI: 10.1016/J.EJRAD.2024.111364

[3] Aqsa Dastgir et al. 'MAFMv3: An automated Multi-Scale Attention-Based Feature Fusion MobileNetv3 for spine lesion classification'. In: *Image and Vision Computing* 155 (Mar. 2025), p. 105440. ISSN: 0262-8856. DOI: 10.1016/J.IMAVIS.2025.105440

[4] Yann Lecun et al. 'Deep learning'. In: *Nature 2015 521:7553* 521 (7553 May 2015), pp. 436–444. ISSN: 1476-4687. DOI: 10.1038/nature14539

[6] Hoi Kwan Lau et al. 'Quantum Machine Learning over Infinite Dimensions'. In: *Physical Review Letters* 118 (8 Feb. 2017), p. 080501. ISSN: 10797114. DOI: 10.1103/PhysRevLett.118.080501

[7] Nathan Killoran et al. 'Continuous-variable quantum neural networks'. In: *Physical Review Research* 1 (3 June 2018). DOI: 10.1103/PhysRevResearch.1.033063

[8] Galan Moody et al. 'Machine learning method for state preparation and gate synthesis on photonic quantum computers'. In: *Quantum Science and Technology* 4 (2 Jan. 2019), p. 024004. ISSN: 2058-9565. DOI: 10.1088/2058-9565/AAF59E

[9] Pranav Kairon and Siddhartha Bhattacharyya. 'COVID-19 Outbreak Prediction Using Quantum Neural Networks'. In: *Advances in Intelligent Systems and Computing* 1279 (2021), pp. 113–123. ISSN: 2194-5365. DOI: 10.1007/978-981-15-9290-4_12

[10] Sophie Choe. 'Continuous Variable Quantum MNIST Classifiers'. In: (Apr. 2022)

[11] Ebrahim Ghasemian et al. 'Quantum machine learning based on continuous variable single-photon states: an elementary foundation for quantum neural networks'. In: *Quantum Information Processing* 22 (10 Oct. 2023), pp. 1–22. ISSN: 15731332. DOI: 10.1007/S11128-023-04137-4/FIGURES/9

[12] Prabhat Anand et al. 'Time-Series Forecasting Using Continuous Variables-Based Quantum Neural Networks'. In: *2024 16th International Conference on COMmunication Systems and NETworkS, COMSNETS 2024* (2024), pp. 994–999. DOI: 10.1109/COMSNETS59351.2024.10427192

Thank you for your attention

dlopez@citedi.mx

Centro de Investigación y Desarrollo de Tecnología Digital (CITEDI-IPN)

Presented at ICE-10 Conference, Valencia, Spain – October 2025